GERMAN - MONGOLIAN INSTITUTE FOR RESOURCES AND TECHNOLOGY

The present work was submitted to
the German-Mongolian Institute for Resources and Technology

INTEGRATING FLOOD MITIGATION AND GROUNDWATER RECHARGE IN WATER SCARCE MINING AREA OF SOUTHERN GOBI MONGOLIA

Bachelor's Thesis

By

TUGULDUR Bat-itgelt

Study program: Environmental Engineer

Student ID: B2100565

1st Supervisor/Examiner: Dr. Ariuntuya Tserendorj

2nd Supervisor/Examiner: Dr. Alireza Arab

Ulaanbaatar/Nalaikh

2025

GERMAN - MONGOLIAN INSTITUTE FOR RESOURCES AND TECHNOLOGY

The present work was submitted to
the German-Mongolian Institute for Resources and Technology

INTEGRATING FLOOD MITIGATION AND GROUNDWATER RECHARGE IN WATER SCARCE MINING AREA OF SOUTHERN GOBI MONGOLIA

Bachelor's Thesis

By

TUGULDUR Bat-itgelt

Study program: Environmental Engineer

Student ID: B2100565

1st Supervisor/Examiner: Dr. Ariuntuya Tserendorj

2nd Supervisor/Examiner: Dr. Alireza Arab

Ulaanbaatar/Nalaikh

2025

Statutory Declaration

Bat-Itgelt, Tuguldur
B2100565

I hereby affirm in lieu of an oath that I provided the submitted bachelor thesis

INTEGRATING FLOOD MITIGATION AND GROUNDWATER RECHARGE IN WATER SCARCE MINING AREA OF SOUTHERN GOBI MONGOLIA

I did not use any sources other than those stated. In case the work is additionally submitted on a data medium, I declare that the written and the electronic form are completely identical. The work was not submitted in the same or similar form to any examination authority.

Nalaikh, 5/28/2025
Place, Date Signature

Acknowledgement

First and foremost, I would like to express my deepest gratitude to my supervisors, Dr. Ariuntuya Tsedendorj from GMIT and Dr. Alireza Arab from TUBAF, for their invaluable guidance, and continuous support, throughout the development of this work. I would also like to sincerely thank Professor Traugott Scheytt from TUBAF for his thoughtful recommendations and genuine concern for my research. A very special thanks goes to Mr. Mohammad Taani, currently pursuing his doctoral degree at TUBAF, for dedicating his time and effort to assist me.

I am deeply grateful to the GMIT scholarship committee for granting me the opportunity to participate in the semester exchange program at TUBAF with a stipend, which allowed me to focus fully on my studies without financial concerns. I am thankful to GMIT students and staff, especially my dear friends who were there for me through the years.

Finally, I extend my heartfelt appreciation to my family, whose unwavering love, encouragement, and belief in me have been the cornerstone of all my achievements. Thank you all for being part of this journey.

Abstract

The Gobi region of Mongolia, characterized by its arid climate and lack of natural groundwater recharge, is increasingly facing intense flash flood events due to climate change. Despite being a dryland, the area experiences short-duration, high-intensity rainfall events that generate destructive runoff. Compounding this challenge, the region's mineral abundance is driving rapid growth in water demand, particularly for mining activities. Groundwater remains the sole water source, yet it is unsustainably extracted without natural replenishment. This thesis investigates a nature-based solution: harvesting flash floodwater to support groundwater sustainability through managed infiltration. A Multi-Criteria Decision-Making (MCDM) approach integrated with the Analytic Hierarchy Process (AHP) was applied using nine thematic layers (slope, soil type, land use, lithology, drainage density, lineament density, rainfall, groundwater depth, and runoff potential) to identify suitable zones for floodwater infiltration across a 1,600 km² study area. The Rational Method was employed to estimate the volume of runoff generated during a 5-year return period rainfall event. The analysis revealed that 35.04 km² (approximately 2%) of the total area is highly suitable for infiltration structures. Within this area, an estimated 1,013,256.86 m³ of floodwater can be harvested and redirected into aquifers per event. The findings support the strategic implementation of infiltration-based structures such as retention basins and recharge ponds to mitigate flood damage and enhance groundwater sustainability in climate-vulnerable, water-scarce mining regions.

Table of content

List of figures

List of tables

List of abbreviations

FSZ - flood susceptible zone
GWRZ - groundwater recharge zone
FRSZ - flood water as recharge suitable zone
MCDM - multi criteria decision making
AHP - analytic hierarchy process
GIS - geographic information system
IDF - intensity duration frequency
AMC - antecedent moisture condition
CN - curve number
SCS - soil conservation service
WOA - weighted overlay analysis
CI - consistency index
TC - time of concentration
LULC - land use land cover
HSG - hydrologic soil group
USDA - united states department of agriculture
FAO - food and agriculture organization
USGS - united states geological survey
NDVI - normalized vegetation index
SRTM - shuttle radar topology mission
DEM - digital elevation model

1. Introduction

A destructive and fast natural hazard, the flash flood in arid regions where it can be even subjected to drought is becoming more frequent while residents in those areas are not fully aware. In the Gobi region, floods occur during the heavy rainfall in the summertime. In that region, rainfall flash floods and mixed mud floods occur as a result of high-intensity rainfall during July and August. However, much of the floodwater either infiltrates into the soil or evaporates within two to three days, limiting its long-term availability for water resources [1].

Mining plays a crucial role in Mongolia's economy, particularly in the Gobi region, where major deposits such as Oyu Tolgoi have attracted large-scale operations. The mining sector accounts for approximately 12.7% of the country’s total water use and is expected to require even more as new projects are developed. Major mines rely heavily on deep, non-potable aquifers and have implemented high-efficiency water recycling systems, reaching up to 85% reuse rates to reduce environmental impacts. However, limited groundwater replenishment continues to pose a serious water management challenge for mining activities in the Gobi region [1][3]. As a result of hydric stress and climate change, rivers, springs and mineral water have been drying up. There are also tensions on water consumption and uses among herding and mining communities, as mining activities use huge amounts of underground water reserves.

Groundwater constitutes around 80% of Mongolia’s total available water resources. Yet, its distribution is highly uneven, with the Gobi region experiencing acute scarcity due to extremely low recharge rates estimated between 0.9 and 2.5 mm per year [2]. The situation is exacerbated by high evaporation and minimal precipitation, making groundwater in this region largely non-renewable. Besides mining, other sectors like agriculture and livestock also exert considerable pressure on the already fragile groundwater reserves, intensifying competition for limited water resources [1]. The main source of water in the arid southern region is groundwater. Unlike the north, surface water sources are scarce [3]. Many of the groundwater aquifers in this region are fossil aquifers, formed under past climatic conditions and receiving minimal recharge from modern precipitation [4]. Recharge in this region is extremely limited, with an annual precipitation of approximately 115–150 mm and an estimated effective recharge rate of only 1 mm per year due to high evaporation and low infiltration rates [4]. Most precipitation-fed water circulates within shallow aquifers (0–20 m depth), while a smaller portion percolates into deeper aquifers (20–50 m and beyond) [7].

The estimated groundwater potential in the Gobi region ranges from 200 to 500 million m³ per year, based on a 25–40-year period of usage and an acceptable decline in groundwater levels of 50–100 meters over this timeframe. The lower estimate of 200 million m³ per year translates to approximately 550,000 m³ per day. Current projections suggest that the available groundwater resources could meet regional water demands for the next 10–12 years. However, this assumption holds only if water consumption remains stable and there are no significant changes in recharge conditions [4, 8]. Proper groundwater management is therefore essential to prevent overexploitation of these fossil aquifers and to ensure long-term water security.

Although the Gobi region is predominantly arid, it is periodically subjected to intense, short-duration rainfall events, resulting in flash floods [4, 7]. These events cause hazardous surface runoff, threatening settlements, infrastructure, and mining operations. These floods have caused significant damage to infrastructure, including electric substations and roads, particularly in areas such as Umnugovi province. Moreover, climate change is expected to increase the frequency and severity of such extreme weather events, further complicating water management efforts in the region. Nevertheless, flash floods also present a potential opportunity: by strategically harvesting and storing floodwater, it may be possible to augment water supplies. Techniques such as constructing artificial catchment areas and using remote sensing to predict flood behavior could enable more sustainable water management. Successful examples from arid regions, where floodwater harvesting integrated with geophysical surveying was used for dam or basin site selection and groundwater recharge assessment, offer valuable insights that could be applied in Mongolia’s Gobi region [5][6]. Several factors influence the occurrence and severity of flash floods in the Gobi region. These include topography (hill slopes), soil and sediment composition, rainfall intensity, and the extent of urbanization [5]. Understanding these factors is crucial for developing effective flood mitigation strategies and ensuring sustainable water management in this vulnerable region.

Recent flash floods [from everyday media]

1. 28th and 29th of September, 2024 at Tsogttsetsii
2. 19th and 20th of July, 2023 at Khanbogd
3. 2nd of August, 2018 at Khanbogd
4. 24th of July, 2024 at Tsogttsetsii

Figure 1.1 Flash flood occurrences in the study area

1.1 Objectives

The primary aim of this study is to develop an integrated approach for sustainable water management in Mongolia's Gobi region, addressing the dual challenges of water scarcity and flash floods. The specific objectives are:

1. To assess the impact of flash floods on infrastructure and communities in the Gobi region using reports and everyday media to get familiar with real life situations in the area where drought and flood occurs at the same time.
2. To evaluate the effects of mining activities on local water resources, focusing on groundwater depletion or dependence on nonrenewable water resources of the activities.
3. To identify and map potential sites for floodwater harvesting using GIS-based Multi-Criteria Decision Analysis (MCDA) adapting research methodology that has been studied and experimented lately.
4. To estimate runoff volumes from historical and projected storm events using the SCS-CN and Rational methods.
5. To propose sustainable water management strategies that integrate floodwater harvesting to support mining operations and local communities with knowledge of the amount of water that can be used for infiltration or retention as well as the resulting ultimate location of that activity.

1.2 Scope and Limitations

This study focused on a catchment area (<2,000 km²) near residential and mining zones (excluding protected areas) with obtainable 2010-2024 weather data, adopting a proven floodwater-to-groundwater recharge suitability mapping method (validated in arid regions like Qatar) combined with standard runoff estimation techniques. While the mixed-methods approach ensured robustness, it required advanced computational expertise and faced constraints from having only one weather station in the study area, necessitating remote sensing data to approximate missing field measurements (e.g., soil properties). The lack of localized prior research further required extrapolating characteristics from global arid-region studies, introducing uncertainties. These compromises balanced feasibility with analytical rigor, though results remain indicative where direct data was unavailable.

2. State of the Art

Recent advances in flash flood mitigation for arid regions have developed sophisticated methodological frameworks that address the unique challenges of data-scarce environments. At the core of these approaches lies the integration of hydrological modeling systems with remote sensing technologies, creating synergistic solutions for risk assessment and mitigation.

The Hydrologic Engineering Center's Modeling System (HEC-HMS) has emerged as particularly valuable for flash flood prediction, employing Muskingum flow routing to simulate complex watershed behavior [35]. This distributed parameter model represents basins as interconnected hydrological elements, allowing for detailed simulation of rainfall-runoff processes even in poorly gauged arid catchments [36]. The system's effectiveness depends heavily on accurate parameterization, achieved through the Soil Conservation Service Curve Number (SC-SCN) method, which estimates runoff based on soil properties and land cover conditions (SCS 1985) [37].

Remote sensing technologies provide critical spatial data inputs for these modeling efforts. Landsat Thematic Mapper (TM) imagery, with its 30-meter resolution in visible

and near-infrared bands, has proven especially useful for land cover classification in arid environments [40]. When combined with field validation and rigorous preprocessing [39], these satellite-derived datasets enable accurate characterization of basin properties essential for both HEC-HMS and SC-SCN applications [42].

Urban areas in arid regions present additional complexities, where conventional stormwater infrastructure is often inadequate. Recent strategies have therefore emphasized alternative approaches including rainwater harvesting systems and community-based early warning programs [43]. These solutions recognize both the hydrological realities of flash flood events and the socioeconomic contexts of vulnerable populations.

Despite these advances, significant challenges remain in model parameterization for heterogeneous arid soils, temporal resolution of satellite data, and integration of local knowledge with technical solutions. The development of more robust validation techniques for ungauged basins represents a particularly pressing research need, as does the improvement of real-time monitoring capabilities in data-scarce regions.[42], [43], [44]. In 2018 around 421 livestocks and 2 people died in severe flood event in the Gobi region within 1 month (2) shown in table 2.1.

Table 2.1 losses caused by flood in 2018 at soums of Umnugobi. Source provided by the military service of Umnugobi.

Soums	Date	Death	Live - stock death	Damaged car	Destroyed household	Destroyed fence and barn	Injured person
Tsogttsetsii	2018.07.24		300				
Bayan ovoo	2018.07.15		21				
Bayan dalai	2018.07.28		100				9
Tsogttsetsii	2018.07.28				1		4
Dalanzadgad	2018.07.28				13	18	55
Dalanzadgad	2018.07.29						4
Tsogttsetsii	2018.08.03			1	1	1	6
Tsogttsetsii	2018.08.03						4

Khanbogd	2018.08.03				1		9
Khanbogd	2018.08.03				1		9
Khanhongor	2018.08.05	1					26

Based on the available data, Oyu Tolgoi mine processed approximately 39.3 million tonnes of ore in 2023. The average water usage per tonne of ore processed was reported to be less than 0.55 cubic meters, with a recycling rate exceeding 85%. [70] This suggests a total water consumption of approximately 15.3 million cubic meters for the year. Assuming continuous operation, this equates to an average pumping rate of about 485.1 liters per second from the deep aquifer.

Oyu Tolgoi has been recognized for its water efficiency, using significantly less water per tonne of ore compared to the global average of 1.2 cubic meters. The mine's water management practices include high-efficiency tailings reclaim, complete reuse of cooling and domestic wastewater, and measures to prevent evaporation, contributing to its high recycling rate.These figures are consistent with the mine's commitment to sustainable water use in the arid South Gobi region, where water conservation is critical [71]. The water used by Oyu Tolgoi is sourced from a deep, saline aquifer and is not suitable for drinking, thereby minimizing impact on local water resources.

2.1 Groundwater Resource Management in Arid Regions

2.1.1 Managed Aquifer Recharge (MAR) Techniques

In the arid regions like the study area the crucial factor for survival and civilization for the living organisms including humans is obviously water. But this precious resource brings not only life but also harm when it's not properly managed or avoided even in this area subjected to drought. There are several management techniques developed lately and from earlier times. Managed Aquifer Recharge (MAR) has emerged as a critical strategy for addressing global water scarcity by intentionally replenishing groundwater reserves through controlled methods [15]. These techniques, which include infiltration basins, recharge wells, and percolation ponds, are particularly valuable in arid and semi-arid regions where surface water availability is highly variable. In Mongolia, where groundwater accounts for over 80% of freshwater withdrawals [16] the Asian Development Bank has identified MAR as a key adaptation

strategy to combat water stress exacerbated by climate change and increasing demand [17].

A specialized form of MAR, known as Flood-Managed Aquifer Recharge (Flood-MAR), has gained attention for its potential to transform floodwaters from a hazard to a resource [18]. This approach captures excess surface water during high-flow events that would otherwise be lost to runoff or cause damage, directing it to suitable infiltration zones. The technique is particularly relevant for Mongolia's flash flood-prone regions, where intense but infrequent rainfall events characterize the hydrological regime.

Several technical approaches have proven effective for Flood-MAR implementation including spreading basins for gradual infiltration in permeable areas [19] injection wells for direct aquifer recharge in suitable geological settings [20], percolation ponds for intermediate storage and natural filtration [21], and recharge trenches and pits for localized infiltration in areas with limited space [22].

Despite its potential, Flood-MAR implementation faces significant challenges in data-scarce environments. As noted by Aloui et al. (2024), much of the uncertainty associated with flash flood utilization stems from inadequate environmental data, including:

1. Real-time flood forecasting limitations
2. Incomplete aquifer characterization
3. Variable infiltration capacity mapping
4. Lack of long-term monitoring systems

These data gaps complicate the identification of optimal recharge sites and the prediction of infiltration rates, particularly in Mongolia's vast and sparsely monitored rural areas [26]. Recent advances in remote sensing and distributed hydrological modeling offer promising solutions to these challenges, though their application in Mongolian contexts remains limited. Mongolia’s unique hydrogeological conditions have spurred several pilot Managed Aquifer Recharge (MAR) projects, each addressing distinct regional challenges. In Ulaanbaatar’s peri-urban Tuul River floodplain (2018–2022), infiltration basins and recharge wells raised groundwater levels by 3.2 m during droughts, though clogging from loess sediments posed challenges [16]. In the Gobi Desert (2019), sand dams and recharge trenches extended water availability by 47 days annually for herders in Dornogovi Province [23]. Meanwhile, the Kharkhorin Flood-MAR pilot (2021) innovatively combined spreading basins with traditional ‘khudag’ wells, mitigating flood damage for 12 households while recharging

8,000 m³/year [29]. These projects demonstrate MAR's adaptability to Mongolia's diverse environments, though site-specific constraints remain.

Flood-MAR holds significant potential in Mongolia due to extreme weather variability, with 73% of flash floods (2018–2022) occurring in areas with suitable aquifers [29]. Successful integration of traditional practices, such as modified khar khuls (ancient diversion channels) in Arkhangai Province, boosted infiltration by 30% [28]). However, 68% of potential sites lack hydrogeological surveys [26], and permafrost thaw disrupts infiltration in northern regions [25]. Key opportunities include high-resolution aquifer mapping in the Gobi, hybrid systems merging modern MAR with traditional khot practices, and policy reforms to incentivize Flood-MAR under revised water laws.

2.1.3 GIS and MCDM for Water Resource Management

The integration of Geographic Information Systems (GIS) with Multi-Criteria Decision-Making (MCDM) techniques has emerged as a robust approach for water resource management, particularly in arid and semi-arid regions. This synergy facilitates the spatial analysis of various environmental and anthropogenic factors, enabling the identification of zones suitable for interventions such as flood control and groundwater recharge.

A pertinent example is the study conducted by Aloui et al. (2024), [12] which applied the Analytic Hierarchy Process (AHP)—a widely recognized MCDM method—within a GIS framework to delineate flood susceptibility zones (FSZ) and groundwater recharge zones (GWRZ) in Qatar. The study considered a comprehensive set of criteria, including topographical factors (elevation, slope, lineament density), hydrological factors (drainage density, rainfall distribution), environmental factors (lithology, soil types, Normalized Difference Vegetation Index), and anthropogenic factors (land use/land cover, stormwater drainage system density). By integrating these layers, the researchers produced spatially explicit maps that identified approximately 64% of the Qatar peninsula as having medium to excellent suitability for aquifer recharge using floodwater. The northern and coastal regions were highlighted as particularly favorable, while urban and southwestern areas were deemed less suitable. The study underscores the potential of GIS-based MCDM approaches in informing sustainable water management strategies in similar arid contexts.[30]

The selection of appropriate criteria is pivotal in MCDM applications [12] emphasized the importance of incorporating factors that significantly influence flood susceptibility and groundwater recharge potential. Their methodology involved a rigorous process of

criteria selection based on data availability and relevance, ensuring a robust analytical framework. The input data were sourced from published maps, remote sensing, and hydrological surveys, enhancing the reliability of the analysis.

The adaptability of the GIS-AHP approach is evident in its application across various geographical contexts. For instance, similar methodologies have been employed in Tunisia's Mornag plain, where eight factors were used to model groundwater recharge potential, revealing that 20% of the area had very high to high recharge potential [30]. In Bangladesh's Barind Tract, an integrated AHP–GIS approach identified four distinct recharge zones, providing valuable insights for sustainable water management [31].

Table 2.2 Groundwater resources in the active mining soums of southern Gobi

Soum name	GW deposit	Total reserves of the deposit (l/sec)	Potential years of use
Khan bogd	Soum center	5.05	25
	Galbiin govi	427.6	25
	Gunii hooloi	921.3	25
	Burgasnii gol	37.0	25

2.2 Floodwater Harvesting Techniques

2.2.1 Global Case Studies (China, Sudan, Egypt)

1. China: Integrated Floodwater Utilization in Arid Landscapes

The northwestern China project demonstrated an innovative approach to transforming flood hazards into resources through engineered desert infiltration systems [32]. The 20 km comb-shaped dam network served dual purposes: flood velocity reduction and controlled water diversion into sandy soils. This system created a cascading water utilization process where floodwaters first infiltrated through desert sediments, emerging as filtered water for domestic and agricultural use. The project's aquaculture integration proved particularly innovative, with continuous water flow through fish ponds (Salmo gairdneri) generating nutrient-rich effluent for crop irrigation while maintaining water quality through natural biofiltration. Satellite monitoring using Sentinel-2 data (10

m resolution NDVI) confirmed significant improvements in surrounding vegetation cover, demonstrating the system's secondary benefits for desertification control [32].

2. Sudan: Flood Risk Assessment and Water Harvesting

In the Sennar Dam region, researchers combined high-resolution topographic analysis with multi-criteria decision making to address both flood risks and water storage needs [33]. The study utilized a 2-meter resolution DEM derived from aerial photography to identify seven potential rainwater harvesting sites while mapping flood vulnerability zones. The methodology assigned weighted values to key factors including land use (0.2), elevation (0.2), topographic wetness index (0.3), and proximity to the Blue Nile (0.3) through expert consultation using the Analytical Hierarchy Process. This approach proved particularly valuable for emergency planning, providing actionable data for dam breach scenarios while identifying sites for future water storage infrastructure development.

3. Egypt: Wadi System Flood Management

The Eastern Desert study by Attwa et al. (2020) [34] presented a comprehensive framework for flash flood utilization in arid wadi systems. By integrating remote sensing data with hydrogeological surveys, the team mapped active flood channels and calculated potential storage capacities for mitigation structures.

Table 2.3 Comparative Analysis of different strategies of flash flood management in similar arid regions.

Region	Primary strategies	Key technologies	Relevance to Mongolia
China	Desert infiltration systems	Sentinel-2 NDVI, AHP weighting	Gobi Desert soil applications
Sudan	DEM-based flood/RWH site mapping	2m aerial DEM, GIS overlay	Ephemeral river management
Egypt	Wadi channel engineering	RS lineament mapping	Flash flood aquifer recharge

The research emphasized the importance of lineament analysis in understanding subsurface water pathways, enabling targeted recharge interventions. Their findings

demonstrated that properly designed check dams could simultaneously mitigate flood hazards while enhancing groundwater recharge rates by up to 40% in test locations.

Lessons for Mongolian Applications

1. China's multi-stage water utilization model could be adapted for the Gobi's alluvial fans, particularly where sandy soils facilitate natural filtration.
2. Sudan's high-resolution topographic approach addresses Mongolia's data scarcity challenges through accessible aerial photography methods.
3. Egypt's wadi studies demonstrate the importance of structural controls for managing sudden flood events in similar arid environments [34].

2.3 Factors Influencing Groundwater and Flash Floods

Groundwater sustainability and flood hazards in arid and semi-arid regions such as the Gobi are influenced by a complex interplay of hydrogeological, climatic, anthropogenic, environmental, and management factors. Understanding these driving elements is critical for developing effective floodwater infiltration mapping and sustainable water management strategies. Previous studies emphasize the need for integrated assessments that account for both natural processes and human interventions [44, 45]. The following subsections detail key categories influencing groundwater unsustainability and flash flood risks.

2.3.1 Hydrogeological Factors

Hydrogeological characteristics fundamentally control groundwater recharge potential and surface runoff behavior. Important parameters include aquifer properties, geological formations, stratigraphy, and the density of rivers and streams [46]. For instance, permeable lithologies such as sandstones enhance infiltration, while impermeable layers like claystones impede recharge and promote surface flooding. Surface runoff dynamics are further influenced by catchment morphology and river network density, affecting how quickly and extensively floodwaters spread across a landscape [47]. In regions like the Gobi, where groundwater often originates from ephemeral flood events, understanding these hydrogeological settings is essential for identifying suitable floodwater infiltration zones.

2.3.2 Climatic Factors

Climatic drivers significantly impact both groundwater availability and flood hazards. Arid climates, characterized by minimal and highly variable rainfall, amplify the importance of capturing and utilizing rare flood events for aquifer recharge [48]. Extreme rainfall episodes—though infrequent—can cause sudden flash floods that result in surface water loss without appropriate management infrastructure [49]. Additionally, rising temperatures, prolonged droughts, and shifting precipitation patterns due to climate change exacerbate water scarcity and flood vulnerability in desert environments. These climatic uncertainties necessitate adaptive strategies for groundwater and floodwater management in future planning efforts.

2.3.3 Anthropogenic Factors

Human activities have increasingly altered natural water systems, aggravating both groundwater depletion and flood risks. Key anthropogenic influences include overgrazing, land degradation, unregulated groundwater abstraction, greenhouse gas emissions, and ecosystem neglect [50]. Infrastructure development, often without regard for hydrological pathways, can further disrupt natural infiltration processes and exacerbate flood risks. Moreover, the absence of flood control and managed aquifer recharge (MAR) systems limits opportunities for sustainable water utilization. In the Gobi region, land-use changes and the lack of integrated water management policies have intensified groundwater stress, highlighting the urgent need for coordinated mitigation measures.

2.4 Research Gaps

Despite advances in understanding groundwater sustainability and flood management, several critical research gaps remain, particularly in arid and semi-arid environments like the Gobi region. Bridging these gaps is essential for developing more effective floodwater infiltration systems, improving groundwater recharge, and enhancing resilience against future climate and land-use changes [51].

2.4.1 Data Needs and Monitoring

A major limitation in current floodwater harvesting and groundwater management efforts is the lack of high-resolution, long-term hydrological and meteorological datasets [53]. Sparse groundwater level monitoring, insufficient flood frequency records, and the limited availability of soil moisture and infiltration data hinder model calibration and decision-making. Remote sensing tools, such as Sentinel-2 NDVI products and high-resolution digital elevation models (DEMs), offer promising alternatives but require ground-truth validation [54]. Without continuous and standardized data collection networks, efforts to design effective MAR systems or flood mitigation strategies remain largely speculative.

2.4.2 Technological Innovation

While traditional flood mitigation structures like check dams and infiltration ponds have demonstrated success, there is a growing need for technological innovations tailored to desert environments. Advanced approaches such as engineered infiltration galleries, bioengineered recharge surfaces, and smart aquifer management systems (using real-time monitoring sensors) are underexplored [55]. Additionally, integrating satellite-based vegetation recovery monitoring and AI-driven hydrological modeling could significantly enhance system design and management, but practical applications in large, remote deserts remain rare [56].

2.4.3 Policy and Implementation

Policy frameworks supporting floodwater harvesting and sustainable groundwater management are often weak, fragmented, or missing in arid regions [57]. In the case of Mongolia’s Gobi Desert, there is limited regulation promoting the dual use of floodwaters for aquifer recharge and surface irrigation. Furthermore, few initiatives actively incorporate stakeholder engagement, local knowledge, or ecosystem-based adaptation strategies into groundwater and flood management plans [58]. There is a pressing need for integrated water resource management (IWRM) policies that not only recognize but actively incentivize the development of MAR infrastructure and sustainable land use practices.

3. Methodology

3.1 Study area

Study area is located in the Southern Gobi Region (SGR) of Mongolia, including the Gunii Khooloi groundwater Basin (43°05'N–43°55'N, 106°10'E–108°05'E), covering approximately 1600 km². The area is in the central asian internal drainage basin. The region have experienced significant economic and population growth due to extensive mining activities.[5-9]

Khanbogd is the second most populated soum after Dalanzadgad, with 8,632 registered inhabitants, but reaching up to 30,000 inhabitants counting the floating population. The settlement experienced rapid growth due to the dynamism of the Oyu Tolgoi mine, the biggest mining project in Mongolia.[10]. The study catchment area was delineated using QGIS GRASS tool.

3.1.1 Location and general setting

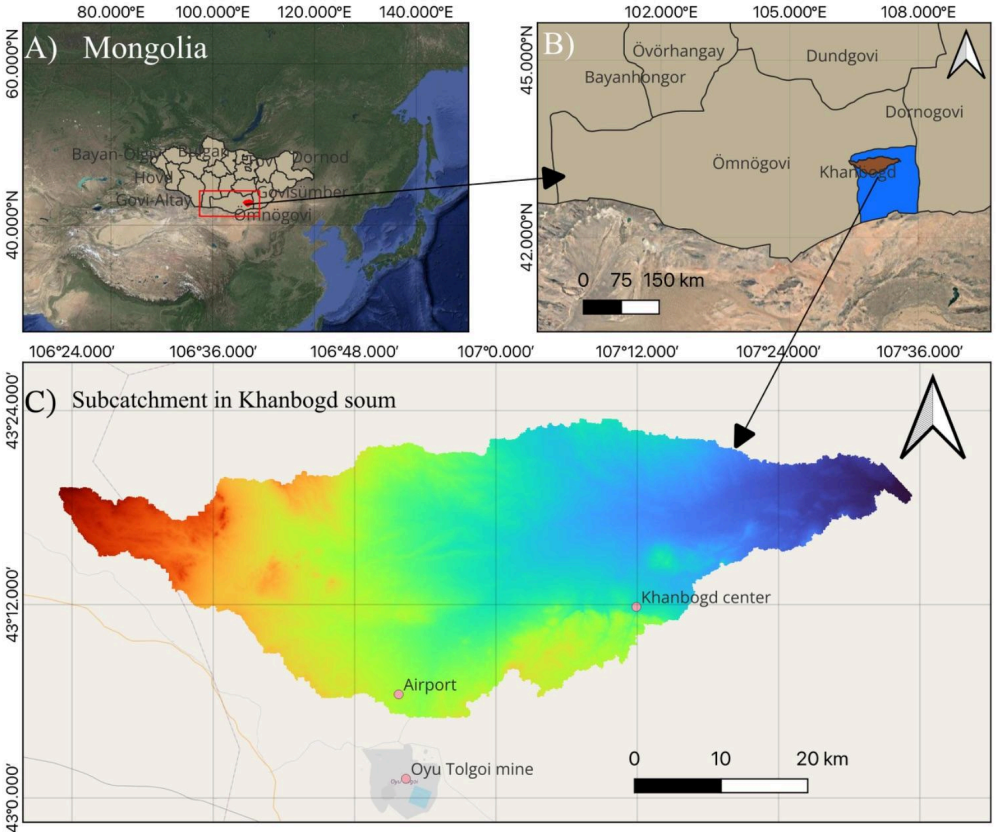

Figure 3.1 Study area A) Mongolia, B) Khanbogd soum, Umnugobi province, C) Catchment area in Khanbogd soum.

The Oyu Tolgoi mine plays a pivotal role in this development. Since 2011, Oyu Tolgoi has implemented policies aimed at fostering a Mongolian supply chain, with a particular emphasis on the South Gobi region.

The rapid expansion of the mining sector has attracted a substantial workforce to Umnugobi, leading to a notable increase in population. This influx has placed considerable strain on urban infrastructure and public services. The province's population has surged from approximately 22,000 in 2018 to around 75,000 in recent years, exacerbating challenges related to housing, education, and healthcare services.

The region’s topography is characterized by arid desert plains, interspersed with uplifted Paleozoic-Mesozoic bedrock and Cretaceous sedimentary basins. Weather conditions and surface flow are mostly dependent on rainfall, intensity, and the structure of soil and soil infiltration rate because, during heavy rains, there is a small flow of dry pebbles occurring in the study area, the Gobi region. 1000–1500 mm of water evaporates from open water. Following the climate zone Köppen–Geiger classification (koppen classifier), this part of Mongolia lies in the dry Bwk (cold desert climate) class, even though the local climate is dry and less precipitation occurs compared to the other regions of the country, with heavy rains and rainwater that contribute in reaching flood levels.

3.1.2 Hydrogeology and geology

The Khanbogd area is located within the Gurvansaikhan island arc terrane, which forms part of the Central Asian Orogenic Belt (CAOB)—a complex assemblage of Paleozoic to Mesozoic subduction and accretionary systems [10]. The region's geological history is marked by significant magmatic and sedimentary events. During the Paleozoic, magmatism was dominated by the emplacement of the Khan Bogd Alkali Granite Pluton (290 ± 1 Ma), a rift-related peralkaline intrusion associated with the Gobi-Tien Shan Rift Zone [11]. Subsequent Mesozoic to Cenozoic periods saw the deposition of sedimentary sequences, with Cretaceous Bayanshiree Series fluvial-lacustrine sandstones and conglomerates, later overlain by Quaternary alluvial deposits.

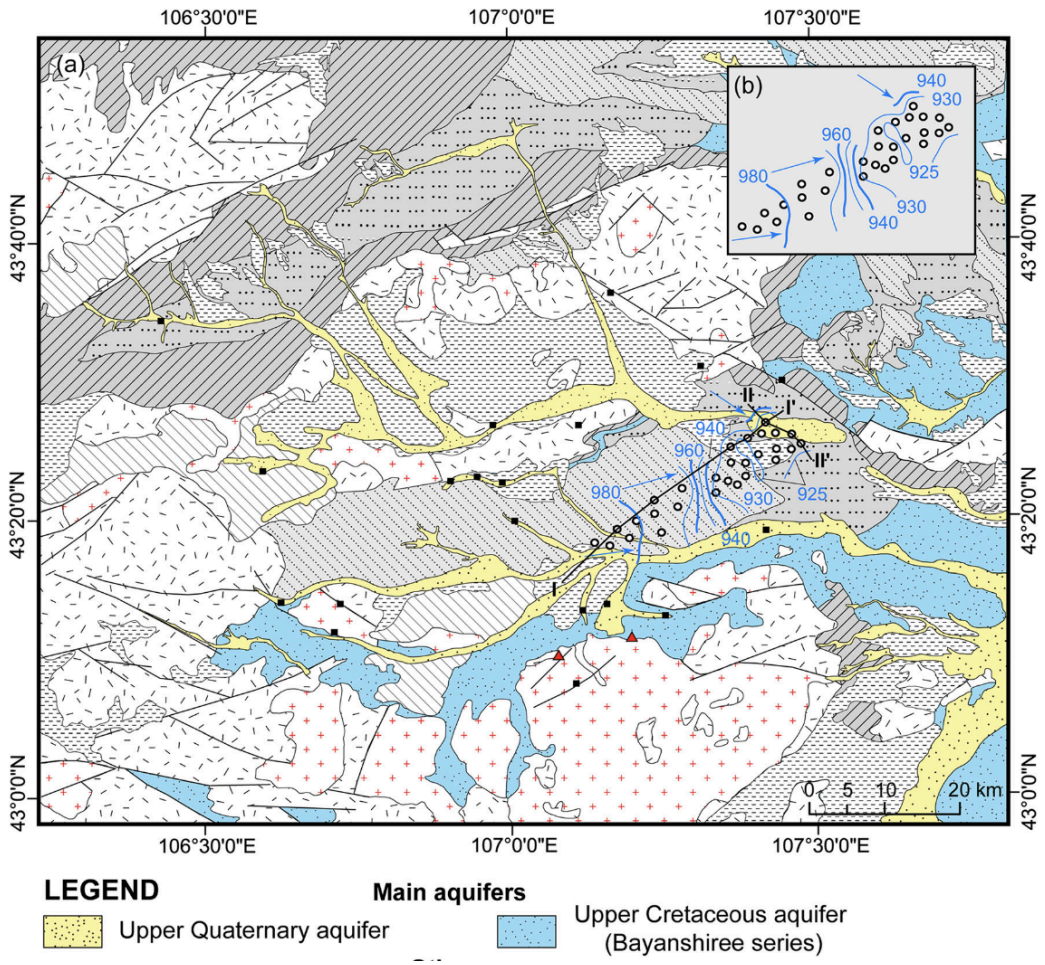

Figure 3.2 a. Hydrogeological map of the southern gobi mongolia, adapted from Koldisheva et al 1986 and Burenkhuu et al. 1995. b. Piezometric map of Gunii Khooloi aquifer from Tudevdorj et al. 2008

The stratigraphy of the Khanbogd area reflects this complex geological evolution. The pre-Carboniferous basement comprises ophiolitic complexes, including mafic volcanic rocks and cherts, exposed near Gashuun Khudag as remnants of Paleozoic oceanic crust. Overlying these are Upper Paleozoic units, notably the 330 Ma island-arc volcanic sequences, which consist predominantly of andesite and basalt derived from Carboniferous subduction processes. This is followed by bimodal rift volcanics around 290 Ma, characterized by basalt, comendite, and alkali granite associations, indicating Permian extensional tectonics. The overlying Cretaceous sedimentary rocks of the Bayanshiree Series consist of sandstone, conglomerate, and siltstone, forming the main deep confined aquifer system. Covering these older units are Quaternary unconsolidated alluvial deposits, composed mainly of sand and gravel, which host the shallow aquifer.

Structural features in the region significantly influence hydrogeological conditions. Fault systems, particularly the NW-SE trending Gobi-Tien Shan Rift faults and NE-SW transverse faults, exert primary control over groundwater flow directions. Additionally, the Khan Bogd pluton's ring dike structures are interpreted as remnants of Paleozoic caldera collapse events, further emphasizing the complex tectonic history of the region [11].

3.2 Research framework

The methodology begins with the collection of secondary data, including geological maps, hydrogeological surveys, precipitation records, soil characteristics, and land-use information. Geographic Information Systems (GIS) are utilized to generate thematic layers for factors influencing flood infiltration and groundwater recharge. A Weighted Overlay Analysis (WOA) and AHP are then applied, assigning relative weights to each criterion based on its importance, to create a composite suitability map identifying optimal floodwater infiltration zones. To estimate floodwater availability, surface runoff volumes are calculated using both the Soil Conservation Service Curve Number (SCS-CN) method and the Rational Method, depending on catchment size and data availability. These runoff estimates are used to assess the potential recharge volumes for managed aquifer recharge (MAR) structures.

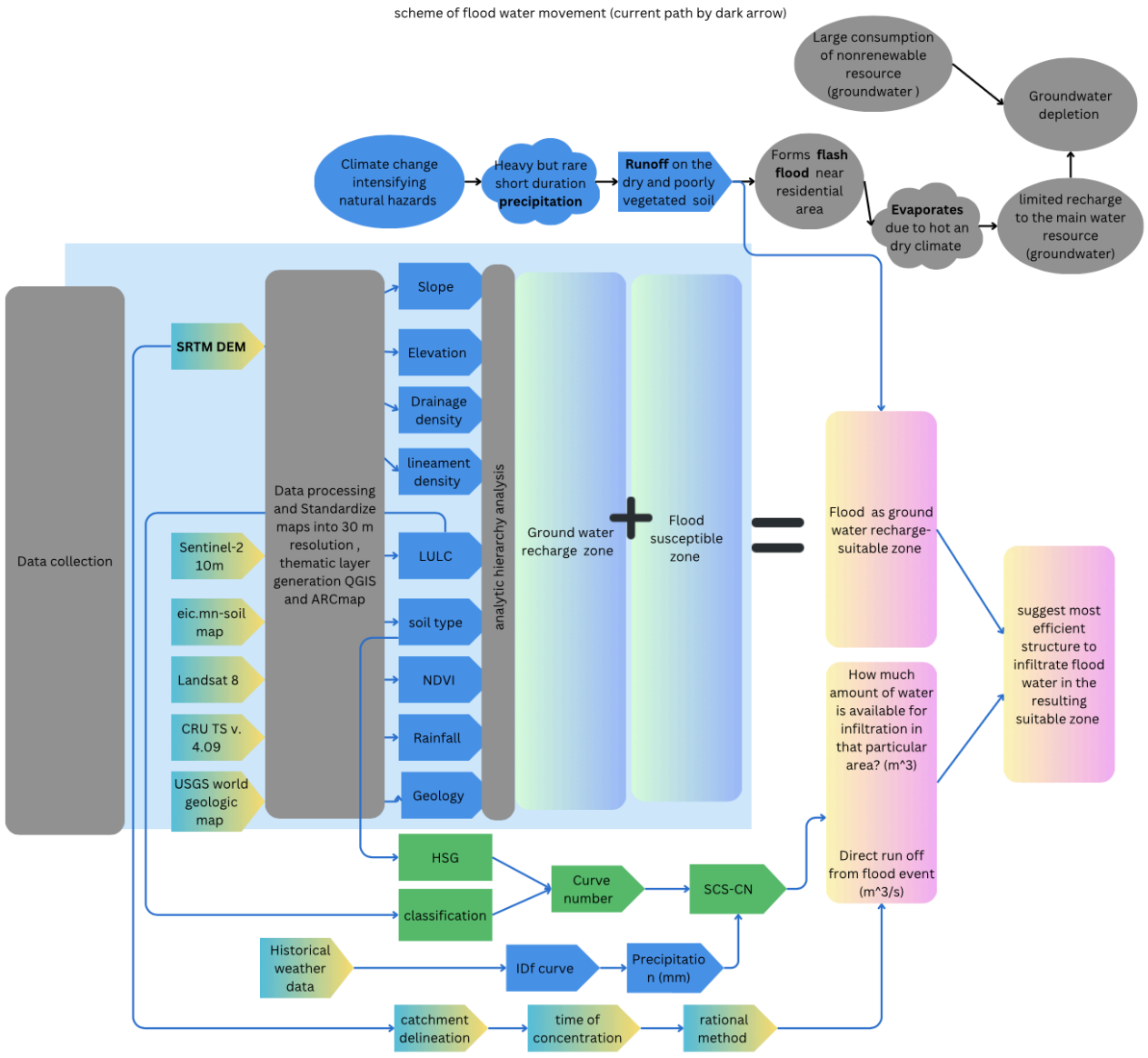

Figure 3.3 Thesis methodology overview diagram

3.3 Flood water infiltration site selection

3.3.1 Influential factors

To identify suitable floodwater infiltration zones, this study employed a GIS-based multi-criteria decision-making (MCDM) approach, following the framework of Aloui et al. (2024) with adaptations for the Gobi region's environmental context. Influential factors were selected based on their hydrological, geological, and environmental relevance to flood infiltration potential. Specifically, **soil** type was included due to its direct control over infiltration capacity, with sandy and loamy soils favoring recharge[61]. **Elevation** and **slope** were selected as key topographic parameters influencing runoff velocity and

ponding potential. **Drainage density** was incorporated to account for surface water concentration and flow paths, with lower densities generally indicating better infiltration opportunities [60] (Equation 3.1).

Geology was considered for its impact on subsurface permeability and aquifer recharge potential [61]. Vegetative cover, represented by the **Normalized Difference Vegetation Index (NDVI**), was included to account for land surface characteristics affecting runoff and infiltration rates [62].

Lineament density, derived through semi-automated detection from high-resolution DEM hillshading, was used as a proxy for subsurface fracturing and permeability [63]. **Precipitation** data from satellite were used to identify areas receiving significant rainfall inputs. **Land use/land cover (LULC)** was considered to avoid bare grounds or impervious areas unsuitable for infiltration [65]. Each thematic layer was standardized, reclassified, and weighted based on expert judgment and regional hydrogeological characteristics to create a composite suitability map for floodwater infiltration.

3.3.2 Data acquisition and pre-processing

All data were standardized into 30 m resolution based on DEM and computational availability after thematic layer creation by clipping mask by layer the study area on QGIS except for rainfall, lineament and drainage density which are processed in arcmap. In order to classify and visualize the data using tools in the processing toolbox, most of the tasks, such as working with plugins and editing attribute tables, were performed manually rather than using semi-automatic or automatic methods

Those input layers were then ranked according to their influence on flood susceptible zone (FSZ) and ground water recharge zone (GWRZ) based on literature review and expert knowledge summarized in table 3.2. And table 3.3 corresponsive.

3.3.3 Multi-Criteria Decision Analysis (GIS-AHP)

After ranking their influence, to get the weights of each factor, a pairwise comparison was performed using Saaty's 1–9 scale for relative importance.

Table 3.1 Data acquisition summary with the sources and published date.

Data	Resolution	Format	Resource	Date
Land use/ cover	10m	Raster	Sentinel-2, ESRI world cover	2024
Landsat-8 satellite imagery (band4 and 5) for NDVI	30m	Raster	Landsat 8 OLI- USGS Earth Resources Observation and Science (EROS) Center	2024
SRTM DEM	30m	Raster	USGS-Earth explorer	2024
Historical weather data	Daily	Tabel	National Agency for Meteorology and Environmental Monitoring	2010-2024
National soil type map	-	Vector	National environmental information centre - geodata catalog	2018
Far asia geologic map	-	Vector	USGS- World geologic map	2021
CN tables	-	Table	Ryu, et al. Development of a Watershed-Scale Long-Term Hydrologic Impact Assessment Model with the Asymptotic Curve Number Regression Equation. Water. 8. 153. 10.3390/w8040153.	2016
Precipitation	0.25° grid'	Raster	Schneider, Udo; Hänsel, Stephanie; Finger, Peter; Rustemeier, Elke; Ziese, Markus : GPCC Full Data Monthly Product Version. Monthly Land-Surface Precipitation from Rain-Gauges built on GTS-based and Historical Data. DOI: 10.5676/DWD_GPCC/FD_M_V2022_025	2011-2020

Table 3.2 Layers/ factors were ranked by their influence on GWRZ based on their infiltration contribution characteristics.

Factors	Rank	Inf	Description/ reasoning
Soil type	1	Most strongly	Directly controls infiltration due to variations in texture, structure, and porosity.
Slope	2		Influences runoff velocity and infiltration; steeper slopes often lead to increased runoff.
Geology	3		Determines subsurface infiltration capacity through lithology and stratigraphy.
LULC	4		Affects surface runoff and infiltration based on vegetation cover and impervious surfaces.
Lineament density	5		Indicates zones of subsurface fracturing that can enhance groundwater recharge by increasing permeability pathways.
Streams density	6		Reflects the concentration of drainage networks; lower stream densities often correspond to better infiltration areas, while high densities suggest surface runoff dominance.
Elevation	7		Indirectly affects infiltration through its control over precipitation patterns, temperature, and erosion processes. Higher elevations might receive more rainfall but also steeper slopes.
Rainfall	8		Provides the primary water input for infiltration. Areas with higher rainfall are prioritized for floodwater harvesting potential.
NDVI	9	Least strongly	Serves as a proxy for vegetation health and density, which influences evapotranspiration and surface permeability. Higher vegetation cover generally indicates better soil structure and infiltration potential.

Table 3.3 Layers/ factors were ranked by their influence on FSZ.

Factors	Rank	Inf	Description/ reasoning
LULC	1	Most strongly	Strongly controls surface runoff generation. Urban and bare lands increase runoff and flood risks, while vegetated areas reduce them through interception and infiltration.
Elevation	2		Influences flow direction and accumulation zones; lower elevation areas are more prone to floodwater accumulation.
Slope	3		Steep slopes promote fast runoff and reduce water retention, while flat areas favor water pooling and increase flood susceptibility.
Geology	4		Governs the infiltration capacity and runoff characteristics depending on rock permeability and structure; impervious lithologies increase flood risk.
Stream density	5		High stream density indicates enhanced surface runoff concentration and greater flood vulnerability.
Rainfall	6		Provides the triggering mechanism for floods; higher rainfall intensity and volume increase flood risk.
Lineament density	7	Least strongly	Fractures may locally affect subsurface drainage, but their impact on surface flooding is secondary compared to other factors.
NDVI	8		Indicates vegetation cover; denser vegetation reduces flood susceptibility through interception and improved soil structure. Sparse vegetation increases runoff.

Soil	9		Affects infiltration rates, but its influence is relatively less direct on surface flood generation compared to topographic and land use factors.

This method involves systematically comparing two factors at a time to judge which one is more influential regarding flood susceptibility or groundwater recharge potential, and by how much. A score of 1 indicates equal importance between two factors, while higher scores represent increasing levels of importance (3 = moderate importance, 5 = strong importance, 7 = very strong importance, and 9 = extreme importance). Conversely, fractional values (such as 1/2, 1/3, 1/5) are used when one factor is less important than the other; for example, 1/3 means that one factor is moderately less important than its counterpart. The resulting comparison matrix was then checked for consistency using the Consistency Ratio (CR) to ensure logical coherence in the judgments using equation 3.6 to 3.9. Final weights for each factor were derived from the normalized eigenvector of the matrix, which were subsequently used in the weighted overlay analysis for site selection equation 3.4 and equation 3.5.

Table 3.4 Sample matrix for finding weights (FSZ) of each input maps using Saaty's 1–9 scale for relative importance.The matrix is reciprocal, meaning if A > B = 5, then B < A = 1/5

Criteria	Soil type	Slope	Geology	LULC	NDVI	Stream density	Elevation
Soil type	1	2	3	4	5	6	7
Slope	1/2	1	2	3	4	5	6
Geology	1/3	1/2	1	2	3	4	5
LULC	1/4	1/3	1/2	1	2	3	4
NDVI	1/5	1/4	1/3	1/2	1	2	3
Streams density	1/6	1/5	1/4	1/3	1/2	1	2

Elevation	1/7	1/6	1/5	1/4	1/3	1/2	1

- Normalization of matrix. Each normalized element:

$$a_{ij}^{norm} = \frac{a_{ij}}{\sum_{i=1}^{n} a_{ij}} \qquad [3.4]$$

where:

a_{ij} = original element at row i, column j

$\sum_{i=1}^{n} a_{ij}$ = sum of the column j

- Eigenvector (priority vector) calculation. Row average (mean of normalized values in each row):

$$w_i = \frac{1}{n} \sum_{j=1}^{n} a_{ij}^{norm} \qquad [3.5]$$

where:

w_i = weight of factor i

n = number of factors

- Consistency check: Find λmax. First, multiply the **original matrix** by the **eigenvector** (weight vector). Then, for each row:

$$\lambda_i = \frac{(Aw)_i}{w_i} \qquad [3.6]$$

Where:

Aw = matrix multiplication of original matrix A and eigenvector w

w_i = corresponding eigenvector value

$$\lambda \text{ max} = \text{average of all } \lambda i \qquad [3.7]$$

- Consistency Index (CI)

$$CI = \frac{\lambda max - n}{n-1} \quad [3.8]$$

- Consistency Ratio (CR)

$$CR = \frac{CI}{RI} \quad [3.9]$$

where:

RI = Random Index (depends on nn)
(example: RI=1.32 for n=7)

3.3.4 Reclassification of maps

Each thematic layer was reclassified based on its properties to standardize the evaluation across different factors. A suitability scale ranging from 1 to 5 was assigned, where a score of 5 indicated the most favorable condition for floodwater infiltration or flood susceptibility, and 1 represented the least favorable. The reclassification was performed using the **Reclassify by Table** tool in QGIS, ensuring that all input layers were transformed into a common suitability scale for the subsequent weighted overlay analysis.

3.3.5 Floodwater Susceptible Zones (FWSZ) and Groundwater Recharge Zones (GWRZ)

After reclassifying each factor by suitability, the Floodwater susceptible Zones (FWSZ) and Groundwater Recharge Zones (GWRZ) were delineated separately.
This was done using the **weights** (Wi) of each influencing factor and the **scores** (Rj) of their properties as reclassified, applied in **QGIS Raster Calculator** according to the following equations:

$$FSZ = \sum_{i=1}^{n} \sum_{j=1}^{m} W_i \times R_J \quad [3.10]$$

$$GWRZ = \sum_{i=1}^{n} \sum_{j=1}^{m} W_i \times R_J \quad [3.11]$$

where :
n = total number of input layers,

m = total number of classes in each layer,
Wi = weight of input layer i,
Rj = rating (score) of class j of layer i.

In QGIS, the **Raster Calculator** was used to multiply each reclassified raster by its corresponding weight and then sum the results to create the final FWSZ and GWRZ maps with the pixel values from 1 being low to 4 being very high for practical interpolation.

3.3.6 Overlay analysis- Flood as resource for groundwater recharge

To identify areas suitable for floodwater-based groundwater recharge, a raster overlay analysis was conducted by combining the Flood Susceptibility Zones (FSZ) and Groundwater Recharge Zones (GWRZ) maps. Both raster layers were initially reclassified into four suitability classes. For the FSZ map, raster pixel values were assigned as follows: 1 for low susceptibility, 2 for medium, 3 for high, and 4 for very high susceptibility. Similarly, the GWRZ map was reclassified with pixel values of 1 for poor recharge potential, 2 for moderate, 3 for good, and 4 for very good recharge potential.

The two reclassified rasters were then multiplied using the raster calculator tool in QGIS, resulting in a new raster layer representing the combined suitability index. The pixel values in the output raster ranged from 1 (1×1) to 16 (4×4), capturing the interaction between flood susceptibility and recharge potential. This multiplication approach helped highlight areas where both conditions flood presence and infiltration opportunity are simultaneously favorable.

The resulting values were reclassified into five floodwater recharge suitability classes: low (≤4), medium (5–6), high (7–9), very high (10–12), and excellent (>12).

3.4 Runoff volume estimation

Runoff volume estimation was conducted to quantify the availability of surface water for potential floodwater harvesting applications. Two methods were applied in this study. First, the Soil Conservation Service Curve Number (SCS-CN) method was used to

estimate runoff depth for a historical storm event with known precipitation depth. Curve Number (CN) values were assigned based on the intersection of hydrologic soil group and land use/land cover data, and applied across the entire catchment to calculate the corresponding runoff depth. Second, the Rational Method was employed to estimate peak runoff and total runoff volume for a projected design storm with a 5-year return period. This approach involved delineating subcatchments, determining their areas, slopes, and flow path lengths, and calculating the time of concentration using the Kirpich equation. Rainfall intensity for each subcatchment was then extracted from an Intensity-Duration-Frequency (IDF) curve based on the computed time of concentration. The resulting runoff volumes provided insight into the spatial distribution of stormwater availability for recharge infrastructure planning.

3.4.1 SCS-CN Method for Historical Storm Event

Since the Curve Number (CN) values for the study area were not readily available, they were estimated through the intersection of two thematic layers: the Hydrologic Soil Group (HSG) map and the Land Use/Land Cover (LULC) map. The HSG map was derived by clipping the global soil map to the extent of the study area, after which the soil types were categorized. Based on these classifications, hydrologic soil group labels were assigned by interpolating from existing literature and regional studies with similar soil characteristics. Simultaneously, the LULC map was developed using remote sensing and classification techniques, and was used in conjunction with soil data to define appropriate CN values. Reference CN values for each soil–land use combination were selected based on standardized lookup tables from the USDA and previous studies conducted in comparable environments. Figure 3.3 presents the CN reference table applied in this study. The classification of hydrologic soil groups (HSGs) in the study area was conducted following the guidelines established by the USDA Natural Resources Conservation Service (NRCS). These guidelines categorize soils into four groups A, B, C, and D based on their infiltration rates and runoff potential. Group A soils are characterized by high infiltration rates and low runoff potential, typically consisting of deep, well-drained sands or gravels. Group B soils have moderate infiltration rates and consist of moderately deep, well-drained soils with moderately fine to moderately coarse textures. Group C soils exhibit slow infiltration rates, often due to a layer that impedes water movement or because of their moderately fine to fine texture. Group D soils have very slow infiltration rates and high runoff potential, commonly comprising clays with high swelling potential, soils with a high water table, or shallow soils over nearly impervious material.

a) b)

Land Use/Land Cover	Hydrological Soil Group			
	A	B	C	D
Annual Crop	67	78	85	88
Brush/Shrubs	30	48	65	73
Built-up	89	92	94	93
Grassland	30	58	71	78
Open Forest	36	60	79	79
Closed Forest	30	55	70	77
Open Barren	63	77	85	88
Perennial Crop	45	66	85	88

Land Use Description	Hydrologic Soil Group			
	A	B	C	D
Commercial, row houses and townhouses	80	85	90	95
Fallow, poor condition	77	86	91	94
Cultivated with conventional tillage	72	81	88	91
Cultivated with conservation tillage	62	71	78	81
Lawns, poor condition	58	74	82	86
Lawns, good condition	39	61	74	80
Pasture or range, poor condition	68	79	86	89
Pasture or range, good condition	39	61	74	80
Meadow	30	58	71	78
Pavement and roofs	100	100	100	100
Woods or forest thin stand, poor cover	45	66	77	83
Woods or forest, good cover	25	55	70	77
Farmsteads	59	74	82	86
Residential 1/4 acre lot, poor condition	73	83	88	91
Residential 1/4 acre lot, good condition	61	75	83	87
Residential 1/2 acre lot, poor condition	67	80	86	89
Residential 1/2 acre lot, good condition	53	70	80	85
Residential 2 acre lot, poor condition	63	77	84	87
Residential 2 acre lot, good condition	47	66	77	81
Roads	74	84	90	92

Figure 3.3 a) CN values of built up area and barren land, b) CN for pasture/ range land were used.

In this study, soil types were identified and categorized based on their texture and composition, as outlined in Table 3.5. For instance, sandy and loose eolian deposits were classified under HSG A due to their high permeability and very low runoff potential. Conversely, sodic and compacted soils, such as brown steppified-desert solonetz, were assigned to HSG D, reflecting their very high runoff potential.

Each soil–land use/land cover (LULC) combination was assigned a Curve Number (CN) value based on standard lookup tables from previous studies conducted in similar environments, such as the USDA NRCS National Engineering Handbook [66] and regional studies [67,69]. Hydrologic soil groups (HSG) ranging from A to D were determined using the Hydrologic Soil Map (HSM) of the world [69] and additional studies in comparable arid and semi-arid areas. After determining CN values for each intersection of LULC and HSG classes for the study area, the weighted CN for antecedent moisture condition II (CNII) was estimated using Equation 3.12. The area (m^2) corresponding to each CN value was calculated using the QGIS statistical tool. Subsequently, CN values for antecedent moisture conditions I (CNI) and III (CNIII) were derived using Equations 3.13 and 3.14, respectively.

Table 3.5 Hydrologic soil groups in the area

Soil type	Brief texture	HSG	Runoff potential
Brown (non division) sandy with brown (non division), eolian deposits	Sandy, loose, eolian	A	Very low
Brown (non division) with eolian deposits, weakly fixed sands	Very loose sands	A	Very low
Brown steppified-desert solonetz	Sodic, compacted, natric	D	Very high
Grey brown desert stony with sairic and weakly fixed sand	Stony + weakly fixed sands	B	Moderate
Shallow stony brown desert-steppe	Shallow, stony	C	High
Typical brown steppe with shallow stony brown steppified-desert	Shallow, stony, mixed	C	High
Typical brown steppified desert with brown (non division) eolian deposits and brown steppified	Mixed sandy/loamy	B	Moderate
Typical brown steppified desert with brown desert-steppe stony and sairic	Compact, stony, possible salinity	D	Very high
Weakly fixed sands	Highly permeable, loose	A	Very low

$$CN_2 = \frac{\Sigma(CN_i \times A_i)}{\Sigma A_i} \quad [3.12]$$

$$CN_1 = \frac{CN_2}{\{2.281 - 0.01281 \times CN_2\}} \quad [3.13]$$

$$CN_3 = \frac{CN_2}{\{0.427 + 0.00573 \times CN_2\}} \quad [3.14]$$

- AMC determination

In arid regions, determining Antecedent Moisture Condition (AMC) is crucial for accurate runoff estimation, especially when using methods like the SCS-CN method. Due to the typical dry conditions in arid areas, AMC is often considered to be AMC-I (dry) for flood simulation. The method used for determining AMC in arid regions often relies on the 5-day rainfall prior to a storm event as a predictor, categorizing AMC into

three levels: AMC-I (dry), AMC-II (normal), and AMC-III (wet). [13, 14], According to known AMC conditions the CN values for each day of the month has been assigned as per AMC.

- Runoff Depth Estimation:

Now that we finally have the complete CN values for each day of the chosen month the following calculations were performed:

Potential Maximum Retention (S): Equation 3.15

$$S = (2540/CN) - 254 \quad [3.15]$$

Initial Abstraction (l_a): Equation 3.16.

$$l_a = 0.2 \times S \quad [3.16]$$

Direct Runoff (Q): Equation 3.17

$$Q = \frac{(P - l_a)^2}{(P + l_a) + S} \quad [3.17]$$

where:
Q = runoff depth (mm) for a single storm event
P = precipitation depth (mm)
l_a = initial abstraction (dimensionless)
S = potential maximum retention (dimensionless)

3.4.2 Rational Method for 5-Year Return Period Runoff Prediction

To estimate future runoff under a 5-year return period storm event, the study area was first divided into hydrological subcatchments based on natural drainage patterns. For each subcatchment, key physical characteristics were derived to support runoff calculation using the Rational Method. The area of each subcatchment was calculated in hectares, the average slope was determined as a percentage from the DEM, and the stream length was extracted from the delineated drainage network. These parameters were later used to estimate the time of concentration and derive rainfall intensity values

from the Intensity-Duration-Frequency (IDF) curve, enabling accurate prediction of peak runoff rates and runoff volumes.

Time of Concentration (Tc) Estimation. The Kirpich equation in watershed lag method is an empirical formula used to estimate the time of concentration (t_c) in a watershed, which is the time it takes for water to travel from the most remote point to the outlet. The formula is as shown in the equation 3.18. **Kirpich Equation** was applied to estimate the **time of concentration** for each subcatchment.

$$T_c = 0.0195 \times (L)^{0.77} \times (S)^{-0.384} \qquad [3.18]$$

Where:

T_c = Time of concentration in minutes.

L = Length of the longest watercourse in meters. This is the distance from the furthest point in the watershed to the outlet.

S = Average slope of the watercourse (dimensionless). This is the difference in elevation divided by the length of the watercourse.

Tc values were computed separately for each subcatchment.

Rainfall intensities (mm/hr) corresponding to the computed Tc were determined using the **Intensity-Duration-Frequency (IDF) curve** derived from historical weather data. For this study, the **5-year return period** storm event was selected.

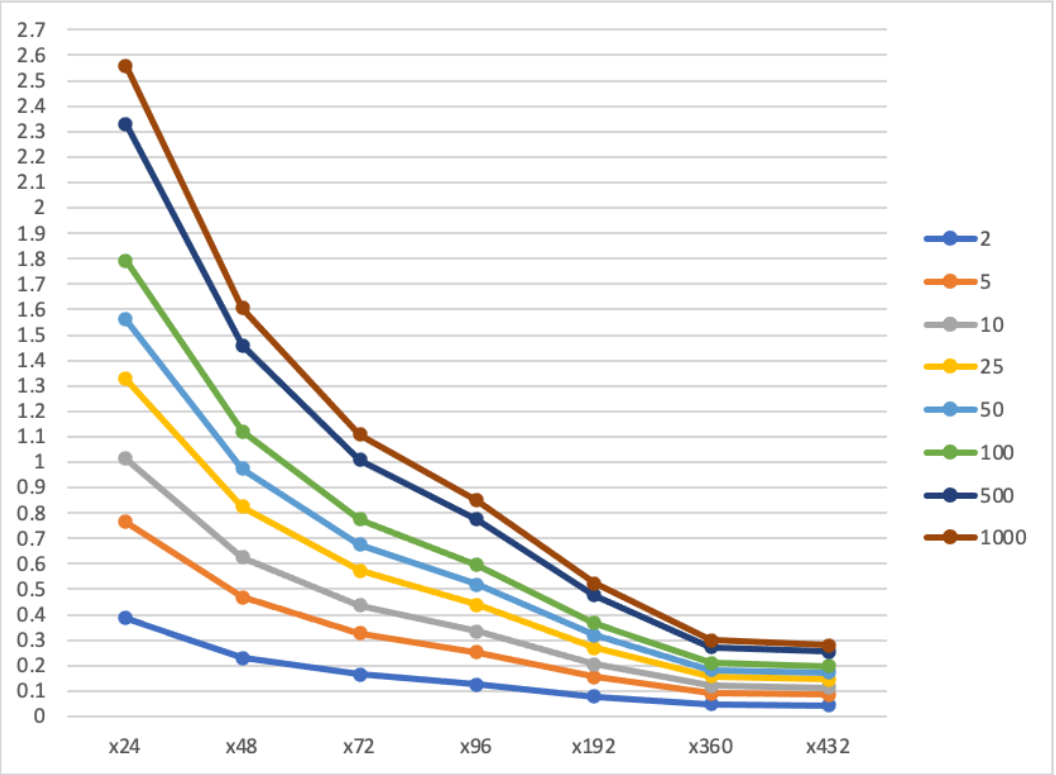

Figure 3.4 IDF curve derived from the historical weather data at station Khanbogd, y axis represents the intensity of rainfall in mm/hour, x axis represents duration of the rainfall event.

The Rational Formula (equation 3.19)was applied for each subcatchment:

$$Q = 0.00278 \times C \times I \times A \qquad [3.19]$$

where:

Q = peak runoff rate (m³/s)

C = runoff coefficient (depends on LULC, optionally from tables)

I = rainfall intensity (mm/h)

A = subcatchment area (ha)

- Runoff coefficient (C)

In this study, runoff coefficients (C) were estimated to evaluate surface runoff potential using the Rational Method. Based on soil texture, land cover, and hydrologic characteristics of the Gobi Region, representative land units were identified, including weakly fixed sands, eolian brown sandy soils, desert-steppe, and solonetz soils. Literature-based coefficient values were assigned to each unit, with midpoints selected from standard runoff coefficient ranges found in

sources such as Rawls et al. (1983) [72], FAO (1998) [73], and Chow et al. (2013) [74].

- The total runoff volume

For each subcatchment was estimated by multiplying the peak runoff rate (Qpeak) obtained from the Rational Method with the storm duration (t). In the absence of a predefined storm duration, the time of concentration (Tc) was adopted as an estimate for the rainfall duration. The runoff volume was calculated using equation 3.20:

$$V = Q \times T_c \times 60 \quad [3.20]$$

Where:

V = volume of the runoff (m^3)

T_c = is expressed in minutes.

4. Result and discussion

4.1 Floodwater Infiltration Site Selection Results

4.1.1 Influential Factor Maps

A total of nine influential factors were considered in the analysis, each mapped individually as shown in Figure 4.1. These factors include slope, elevation, soil type, land use/land cover (LULC), NDVI, geology, drainage density, lineament density, and precipitation. To evaluate their relative importance in determining flood susceptibility and groundwater recharge potential, the Analytic Hierarchy Process (AHP) was applied. The resulting weights for each factor are presented in Table 4.1, along with the calculated Consistency Index (CI) and Consistency Ratio (CR) to validate the reliability of the pairwise comparison matrix. A higher weight indicates a greater influence of that factor in the final suitability analysis, guiding the classification and overlay of thematic layers in subsequent steps.

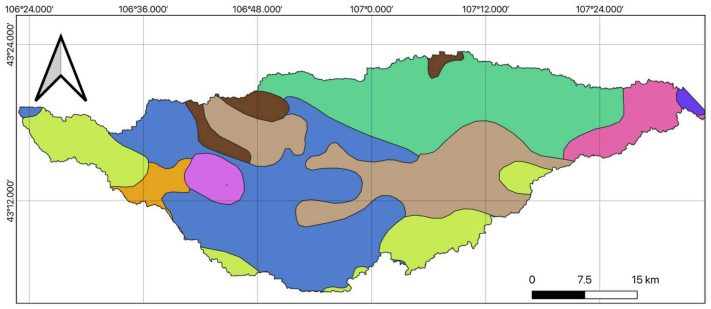

soil_catchment
- Brown (non division) sandy with brown (non division), eolian deposits
- Brown (non division) with eolian deposits, weakly fixed sands
- Brown steppified-desert solonetz
- Grey brown desert stony with sairic and weakly fixed sand
- Shallow stony brown desert-steppe
- Typical brown steppe with shallow stony brown steppified-desert
- Typical brown steppified desert with brown (non division) eolian deposits and brown steppified
- Typical brown steppified desert with brown desert-steppe stony and sairic
- Weakly fixed sands

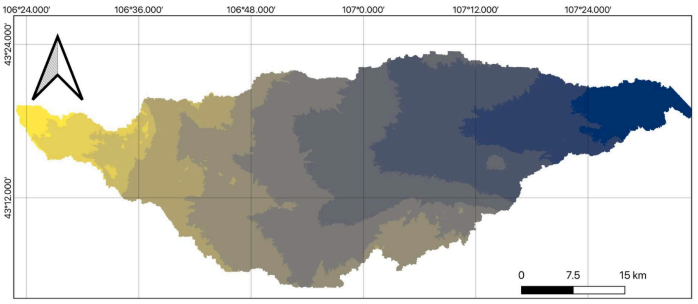

Elevation Band 1
- <= 1000
- 1000 - 1050
- 1050 - 1100
- 1100 - 1150
- 1150 - 1200
- 1200 - 1250
- 1250 - 1300
- 1300 - 1350
- 1350 - 1400
- > 1400

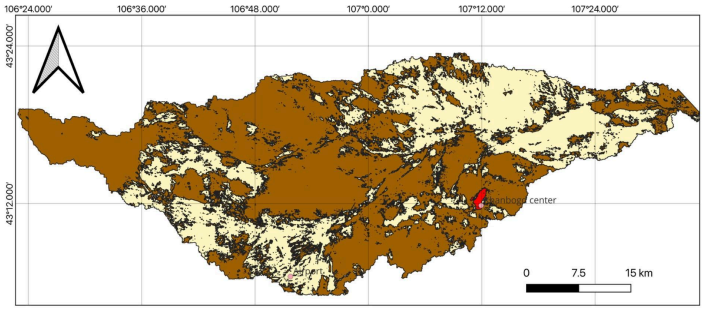

- Developed sites

Land use/ cover
- Bare Ground
- Built_Area
- Range_Land

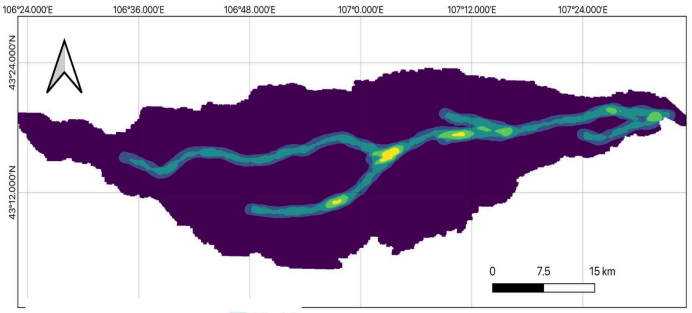

Drainage density (km/km^2)
Band 1
- <= 0.3
- 0.3 - 0.7
- 0.7 - 1.0
- 1.0 - 1.3
- > 1.3

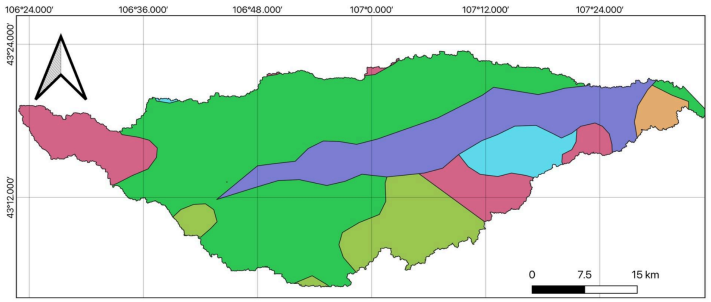

Geology
- Carboniferous
- Cretaceous
- Cretaceous/ Jurasic
- Permian
- Quaternary
- Undivided Tertiary

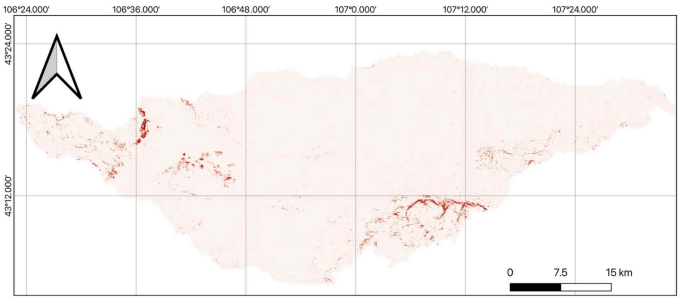

Slope Gradient %
- <= 5
- 5 - 8
- 8 - 13
- 13 - 17
- > 17

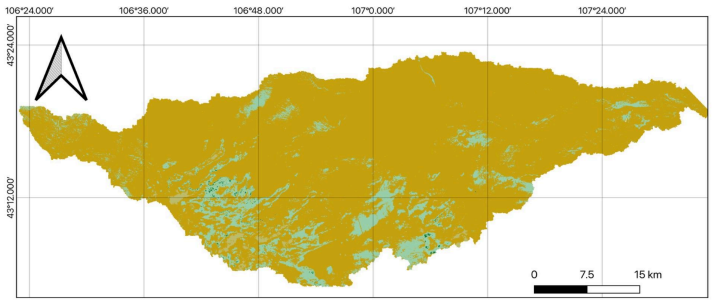

NDVI
- <= -0.2
- -0.2 - 0
- 0 - 0.05
- 0.05 - 0.1
- > 0.1

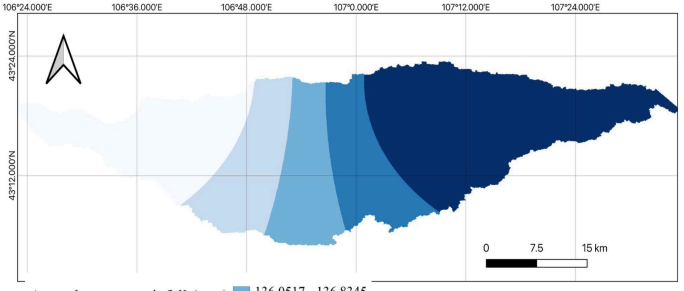

Annual average rainfall (mm)
Band 1 (Gray)
- <= 135.2689
- 135.2689 - 136.0517
- 136.0517 - 136.8345
- 136.8345 - 137.6172
- > 137.6172

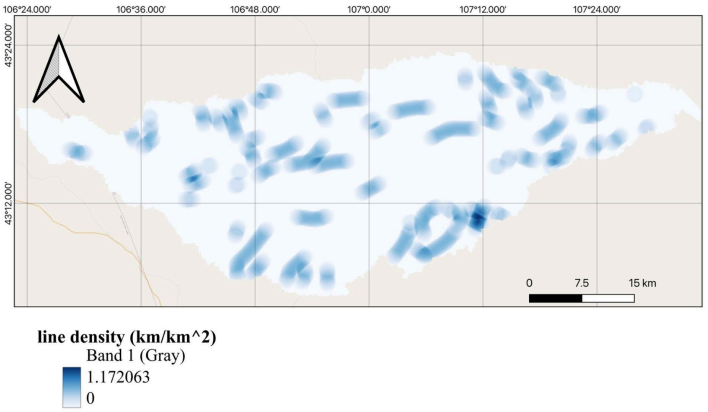

Figure 4.1 Thematic maps for the visual interpolation of flood water infiltration/harvesting suitability mapping: **(a)** Soil type, **(b)** Elevation /m/, **(c)** Land use/ cover, **(d)** Stream density , **(e)** Geology, **(f)** Slope gradient /%/, **(g)** NDVI, **(h)** Lineament density, **(g)** Annual average rainfall.

4.1.2 Multi-Criteria Decision Analysis (AHP Results)

For the groundwater recharge zone (GWRZ) analysis, the highest weight was assigned to soil type (0.3070), followed by slope (0.2182), geology (0.1543), and land use/land cover (LULC) (0.1089), reflecting their strong influence on infiltration capacity.

Table 4.1 Weights for FSZ and GWRZ

Layer	GWRZ weight (x100%)	FSZ weight (x100%)
Soil	0.3070	0.0189
Rainfall	0.0259	0.0533
Slope	0.2182	0.1543
Geology	0.1543	0.1089
LULC	0.1089	0.3070
Lineament	0.0764	0.0370
Stream Density	0.0533	0.0764
Elevation	0.0370	0.2182
NDVI	0.0189	0.0259

In contrast, the flood susceptibility zone (FSZ) analysis ranked LULC as the most significant factor (0.3070), followed by elevation (0.2182) and slope (0.1543), emphasizing the importance of surface characteristics in runoff generation. The

complete weights for both analyses are presented in Tables 4.1. The consistency of the pairwise comparison matrices was validated using the Consistency Ratio (CR), which was calculated as 0.035 in both cases—well below the acceptable threshold of 0.1. This confirms that the weightings are logically consistent and reliable for further spatial analysis. To evaluate the reliability of the pairwise comparisons in the Analytic Hierarchy Process (AHP), a consistency check was performed. The maximum eigenvalue (λmax) was calculated as **9.41**, resulting in a **Consistency Index (CI)**of **0.051**. The **Consistency Ratio (CR)** was computed as **0.035**, which is well below the generally accepted threshold of **0.1**. This indicates that the judgments made during the pairwise comparisons are consistent and the weighting results are valid for use in the multi-criteria decision analysis.

4.1.3 Reclassified Thematic Layers

Each of the nine thematic layers was reclassified into five suitability classes to support the weighted overlay analysis for both Flood Susceptibility Zones (FSZ) and Groundwater Recharge Zones (GWRZ). Elevation values in the study area ranged from approximately 1000 to 1400 meters above sea level. To standardize the classification, the 400-meter range was divided into five equal intervals, assigning the highest suitability score (5) to the lowest elevation range (1000–1080 m) and the lowest score (1) to the highest elevation range (1320–1400 m), assuming lower elevations are more prone to water accumulation and potential infiltration. Slope was similarly reclassified, with flatter areas (0–5%) receiving the highest score (5) due to their low runoff velocity and higher infiltration potential, and steeper slopes (>17%) receiving the lowest score (1). Soil types were ranked based on their permeability and structure, where weakly fixed sands and sandy eolian deposits were given the highest suitability score (5), while compacted or sodic soils such as brown steppified-desert solonetz received the lowest (1), reflecting their limited infiltration capacity. Geologic formations were evaluated based on porosity and permeability, with unconsolidated Quaternary deposits rated highest (5) and compact Carboniferous formations rated lowest (1). Land use and land cover (LULC) classes were assigned scores based on their influence on surface sealing and infiltration: rangelands were scored highest (5), bare soil moderately (3), and urban/road areas lowest (1). NDVI values, used as a proxy for vegetation density, were classified into five ranges, with higher vegetation cover (NDVI > 0.6) assigned the

highest score (5), indicating better soil structure and infiltration. Drainage density was evaluated by proximity to streams, assuming areas closer to streams are more affected by surface runoff and thus scored higher for FSZ. Rainfall and lineament density were both reclassified into five suitability classes based on value ranges, where higher precipitation and greater fracture density were assigned higher scores due to their relevance to both flood susceptibility and recharge potential. The full set of reclassified scores is presented in Table 4.2, where a score of 5 represents the most suitable condition and 1 the least suitable, consistent across both FSZ and GWRZ analyses.

Table 4.2 Assigning scores for the properties of layers from 5 being most suitable to 1 being least for FSZ similar with GWRZ

Factors	**Components**	**Reclassified by suitability/ score/**
Soil type	• Weakly fixed sands • Brown (non division) sandy with brown (non division), eolian deposits • Shallow stony brown desert-steppe • Typical brown steppe with shallow stony brown steppified-desert • Typical brown steppified desert with brown (non division) eolian deposits and brown steppified • Typical brown steppified desert with brown desert-steppe stony and sairie • Grey brown desert stony with sairie and weakly fixed sand (**Sandy Clay Loam USDA**) • Brown steppified-desert solonetz	5 5 5 4 3 2 1 1
Slope	0–5% 5–8% 8–13% 13–17% 17%-inf	5 4 3 2 1

Geology	● Quaternary (Unconsolidated sand, gravel, alluvium) ● Undivided Tertiary (Mixed: sandstone, claystone, tuff, volcanic) ● Cretaceous (Sandstone, shale) ● Cretaceous–Jurassic (Sandstone, limestone, some shale) ● Permian (Sandstone, marl, evaporites, limestone) ● Carboniferous (Often coal, shale, compact sandstone, limestone)	5 4 3 3 2 1
LULC	Range land Bare soil Urban/roads	5 3 1
NDVI	NDVI > 0.6 0.4–0.6 0.2–0.4 0.0–0.2 < 0.0	5 4 3 2 1
Streams density	Greater than 1.3 km/ km^2 1.0 - 1.3 km/ km^2 0.7 - 1.0 km/ km^2 0.3 - 0.7 km/ km^2 0 - 0.3 km/ km^2	5 4 3 2 1
Elevation	1000m - 1080m 1080m - 1160m 1160m - 1240m 1240m - 1320m 1320m - 1400m	5 4 3 2 1
Rainfall (Annual average)	Greater than 137.6 mm 136.8 - 137.6 mm 136.0- 136.8 mm	5 4 3

	135.2- 136.0mm Less than 135.2mm	2 1
Lineamen t density	0.8 - 1.17 km/ km ^{2} 0.6 - 0.8 km/ km ^{2} 0.4 - 0.6 km/ km ^{2} 0.2 - 0.4 km/ k ^{2} 0 - 0.2 km/ km ^{2}	5 4 3 2 1

To derive suitability maps for Groundwater Recharge Zones (GWRZ) and Floodwater susceptible Zones (FSZ), a Weighted Overlay Analysis (WOA) was conducted using the following formula:

GWRZ Suitability Index (GSI):

GSI=(0.3070×Soil)+(0.0259×Rainfall)+(0.2182×Slope)+(0.1543×Geology)+(0.1089×LULC)+(0.0764×Lineament)+(0.0533×Stream Density)+(0.0370×Elevation)+(0.0189×NDVI)

FSZ Suitability Index (FSI):

FSI=(0.0189×Soil)+(0.0533×Rainfall)+(0.1543×Slope)+(0.1089×Geology)+(0.3070×LULC)+(0.0370×Lineament)+(0.0764×Stream Density)+(0.2182×Elevation)+(0.0259×NDVI)

Each layer was reclassified into suitable classes before overlay, and the sum of weights for each formula equals 1.0, ensuring proper normalization. The final suitability maps were generated by applying these formulas in GIS software.

4.1.4 Floodwater Spreading Zones (FWSZ) and Groundwater Recharge Zones (GWRZ) GIS-AHP

The Flood Susceptibility Zone (FSZ) map was classified into five classes based on composite scores from the weighted overlay analysis: very low susceptibility (≤ 1.8),

low (1.8–2.6), moderate (2.6–3.4), high (3.4–4.2), and very high (> 4.2). As shown in Figure 4.2, areas with high to very high flood susceptibility (orange and dark brown colors, scores above 3.4) are predominantly located in the central and eastern parts of the study area. These regions are generally flatter with lower elevation and closer to drainage networks, making them more prone to surface water accumulation and runoff concentration. The moderate susceptibility zones (yellow, 2.6–3.4) form a transitional belt surrounding the high-risk core and extend into southern and western areas, where topographic and land cover conditions are mixed. Areas with low to very low flood susceptibility (green and blue, < 2.6) are mainly observed in the northwestern and southwestern corners of the catchment. These zones are typically characterized by steeper slopes, higher elevations, and coarser soil textures, which contribute to faster runoff and reduced water retention. This spatial distribution supports the identification of flood-prone areas that may be suitable for floodwater spreading or require protection measures.

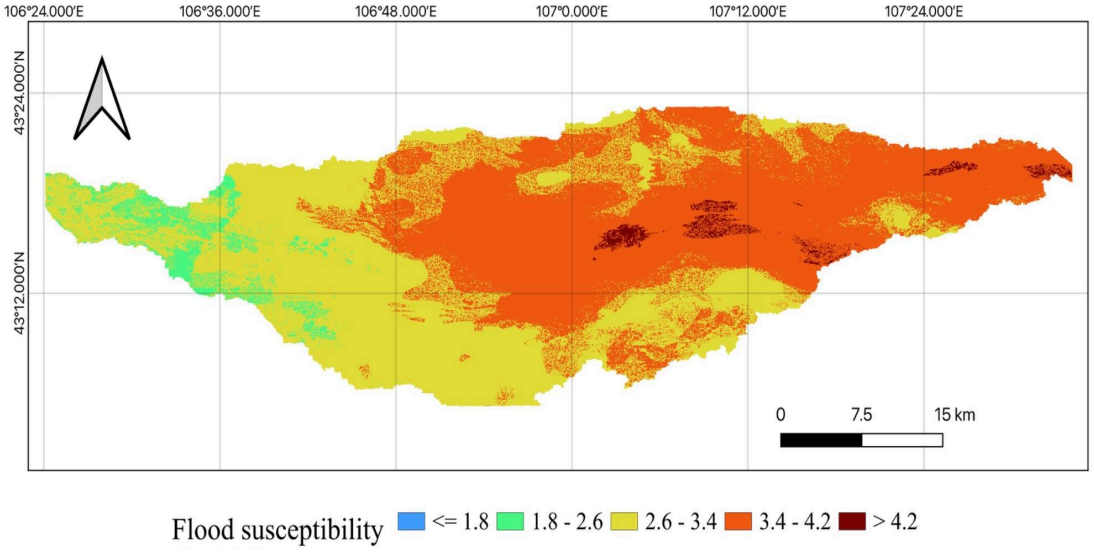

Figure 4.2 Flood susceptibility of study catchment area based on GIS-AHP mapping

The final Flood Susceptibility Zone (FSZ) map was classified into four main categories ranging from most unsuitable to most suitable, based on the weighted overlay of contributing factors such as slope, elevation, drainage density, and land cover. Out of the total 1731.01 km² study area, the largest portion—approximately 962.10 km² or 55.6%—was categorized as moderate susceptibility (class 3), followed by 732.52 km² (42.3%) under the moderate to high susceptibility class (class 4). A small portion of the area, only 36.28 km² (2.1%), fell into the most unsuitable zone (class 2), which includes

high-elevation or steep-sloped regions with low flood risk. Notably, only 0.12 km² (less than 0.01%) was classified as most suitable (class 5) for floodwater accumulation, indicating limited natural depressions or low-slope areas optimal for surface water retention. These results highlight that while a significant portion of the catchment is moderately prone to flooding, zones with high floodwater spreading potential are extremely scarce and must be carefully targeted for harvesting interventions.

The GWRZ map was classified into five recharge potential categories based on the weighted overlay analysis scores: very low (≤ 2.5), low (2.5–3.0), moderate (3.0–3.4), high (3.4–3.9), and very high (> 3.9). As illustrated in Figure 4.3, the areas with very high recharge potential (dark brown, > 3.9) are predominantly concentrated in the central and southeastern parts of the study area, forming continuous zones that coincide with flatter topography and favorable geological conditions. The high recharge zones (orange, 3.4–3.9) surround the core high-potential areas and extend toward the eastern and southern regions, reflecting transitional zones with moderately suitable infiltration properties. Moderate recharge potential (light green, 3.0–3.4) is more evenly distributed, particularly in the central and southern belts, indicating mixed land cover and soil characteristics.

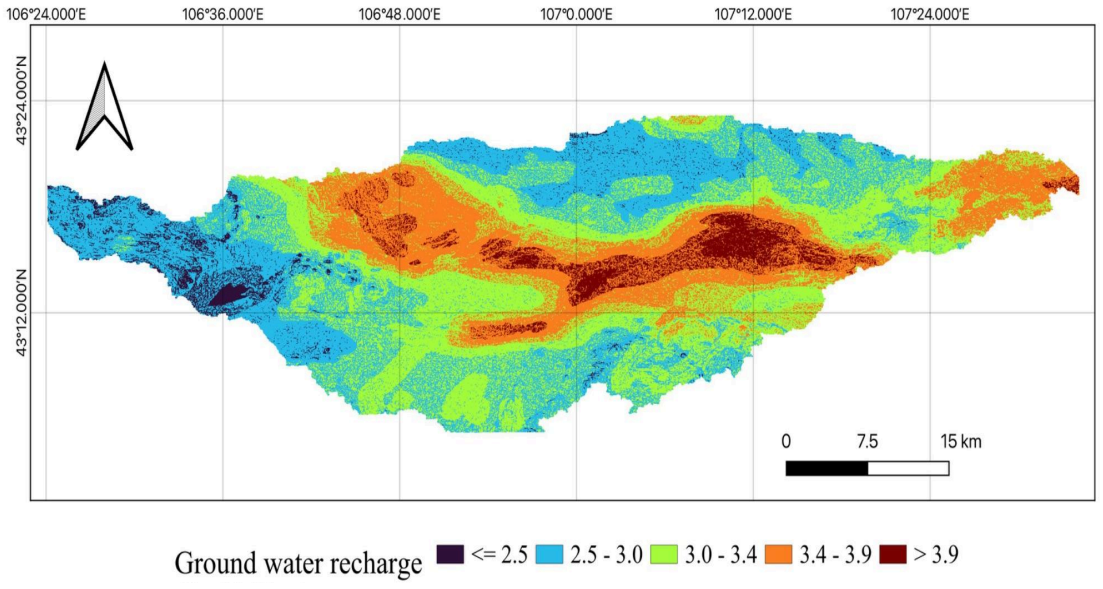

Figure 4.3 Ground water recharge zone of study catchment area based on GIS-AHP mapping

In contrast, the low to very low recharge zones (blue and purple, < 3.0) are mostly located in the northwestern and western edges of the catchment, where steep slopes, stony terrain, or compacted soils reduce infiltration capacity. These spatial patterns highlight the heterogeneity of recharge potential within the study area and provide essential guidance for prioritizing floodwater harvesting interventions.

The final Groundwater Recharge Zone (GWRZ) map was initially derived using five suitability classes based on the weighted overlay of thematic layers. However, for clarity and ease of interpretation, the classified raster was consolidated into three main classes: most suitable, moderate, and poorly suitable. This simplification was made to better distinguish practical groundwater recharge potential zones and to facilitate decision-making for regional planning. The total area of the study region is approximately 1730.78 km². Of this, 411.26 km² (about 23.8%) was categorized as most suitable for groundwater recharge, typically representing areas with favorable soil types, high permeability geology, and low slopes. The moderate suitability zone covered the largest area, 1270.26 km² or 73.4%, reflecting generally good recharge conditions with some limiting factors. Only 49.26 km², or 2.8%, was classified as poorly suitable, often due to compacted soils, steep terrain, or low infiltration potential. These spatial results offer valuable guidance for prioritizing areas for managed aquifer recharge development in the Gobi region.

4.1.5 Overlay Analysis Results

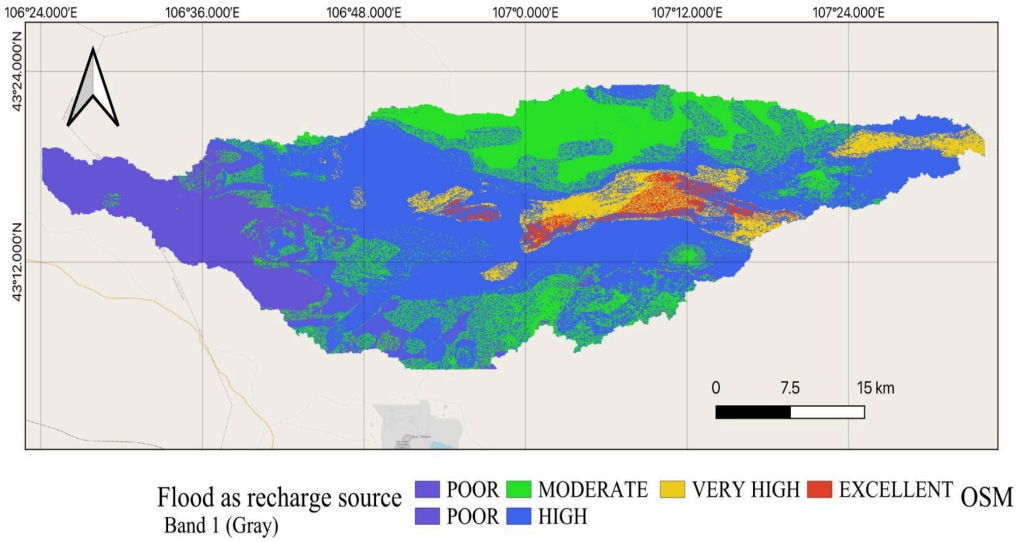

Figure 4.4 Flood water as groundwater recharge suitability map

The final Floodwater Recharge Suitability Zone (FRSZ) map was produced by overlaying the Flood Susceptibility Zone (FSZ) and Groundwater Recharge Zone (GWRZ) maps. Each raster was reclassified into four classes representing flood and recharge potential, and then multiplied using QGIS's raster calculator. The resulting values were reclassified into five suitability categories: poorly suitable, moderately suitable, highly suitable, very highly suitable, and excellent. As shown in Figure 4.4, the majority of the study area, approximately 884.74 km² (51.1%), was classified as highly suitable, representing areas with a favorable overlap between surface water accumulation and infiltration potential. Moderately suitable zones covered 423.91 km² (24.5%), while poorly suitable zones accounted for 288.02 km² (16.6%), primarily located in the northwestern and southern margins of the catchment. Very highly suitable areas made up 98.03 km² (5.7%), and the excellent suitability class, comprising only 35.04 km² (2.0%), was limited to central low-lying regions with strong potential for floodwater harvesting and recharge. These spatial results can help inform future site selection for managed aquifer recharge projects in the Gobi region. Discuss which areas are most suitable for dual-purpose (flood spreading and recharge).

4.2 Runoff Volume Estimation Results

4.2.1 SCS-CN Runoff Estimation for Historical Event

The Curve Number (CN) values were determined through the intersection of the Land Use/Land Cover (LULC) map and the Hydrologic Soil Group (HSG) layer. Based on the CN values provided in Table 4.3, the average CN for Antecedent Moisture Condition II (CN_2)—which applies when the 5-day cumulative precipitation is between 13 mm and 28 mm—was calculated as **80.36**. This value is typically used under normal soil moisture conditions. Additionally, CN values were adjusted for other moisture conditions using standard SCS conversion formulas. The resulting value for **CN_1**, applicable when the 5-day cumulative precipitation is less than 13 mm (dry conditions), was **64.20**, while **CN_3**, representing wet conditions with more than 28 mm of rainfall in the past 5 days, was calculated as **90.55**. These values reflect the average runoff potential of the study area under varying moisture conditions and were subsequently used in the SCS-CN runoff estimation model.

Table 4.3 Interpolated CN table in the study area

Land use type	Hydrologic soil group			
	A	B	C	D
Built up area	89	92	94	93
Bare ground	63	77	85	88
Range land	68	79	86	89

Based on historical weather data, a single flood event was identified, and the corresponding runoff depth was calculated using the SCS Curve Number (CN) method. According to Table 4.4, the five-day cumulative precipitation preceding the event was 18.24 mm, which corresponds to Antecedent Moisture Condition (AMC) Type II. Consequently, the CN value for AMC Type II was selected. After determining the appropriate CN, the potential maximum retention (S) was calculated, as shown in Table 4.4. The resulting runoff depth for this event was calculated to be 63.09 mm. This value can be further used to estimate the total runoff volume for the entire area. This calculation serves to validate the result obtained using the Rational Method.

Table 4.4 runoff depth of the single storm event (extracted from historical weather data)

Date	Precip (mm)	4 days cumulative precipitation	AMC	CN	S	Runoff depth
2018- 08-01	0	-	-	-	-	-
2018- 08-02	1.803	-	-	-	-	-
2018- 08-03	7.798	-	-	-	-	-
2018- 08-04	8.636	-	-	-	-	-
2018- 08-05	33. 641	18.24	2	80.36	62.08	63.09

4.2.2 Rational Method Runoff Prediction for 5-Year Return Period

For each sub-catchment in the study area, key hydrological parameters—such as stream length, catchment area, and average slope—were determined to estimate the time of concentration using the Kirpich formula. Based on the calculated time of concentration and the 5-year return period Intensity-Duration-Frequency (IDF) curve derived from historical meteorological data, rainfall intensity values were obtained. Using the Rational Method, the peak discharge (Q) was calculated for each

sub-catchment by incorporating an average runoff coefficient of 0.29. The results, including runoff volume for each sub-catchment, are summarized in Table 4.5.

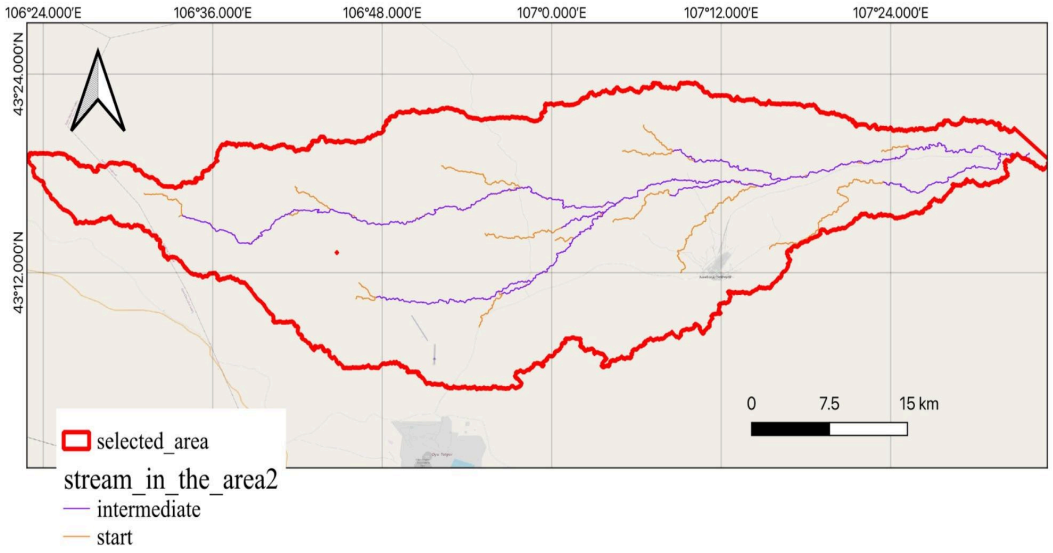

Figure 4.5 Streams in the study area

Table 4.5 Runoff volume in the each sub catchment area

subcatchment ID	1	2	3	4	5	6
Stream length (m)	87242.4	104834.1	83556.1	62469.8	134432.8	53835.5
Average Slope %	2					
Time of concentration (min)	95.1	109.6	92.1	73.6	132.8	65.6
Intensity (mm/hour)	0.77	0.65	0.77	0.95	0.55	1.1
Area (ha)	33682.9	41793.3	34584.1	18238.9	17236	28637.6
Average runoff coefficient	0.6					
Q (m^3/s)	43.2	60.4	59.2	38.5	21.1	70
runoff volume m^3	246830.3	397085.2	326864	170006.3	167812.8	275631.5
total possible water amount m^3	1140785.8					

Based on the floodwater recharge zone (FRZ) suitability map, only sub-catchments 1 through 4 contribute flow into suitable infiltration areas. Thus, the estimated runoff volume available for infiltration from these catchments is: Infiltration-Eligible Runoff=119,301.33+397,085.22+326,864.03+170,006.27=1,013,256.86 m³

Conceptual model for flash flood and groundwater depletion influencing factors and solution possibility

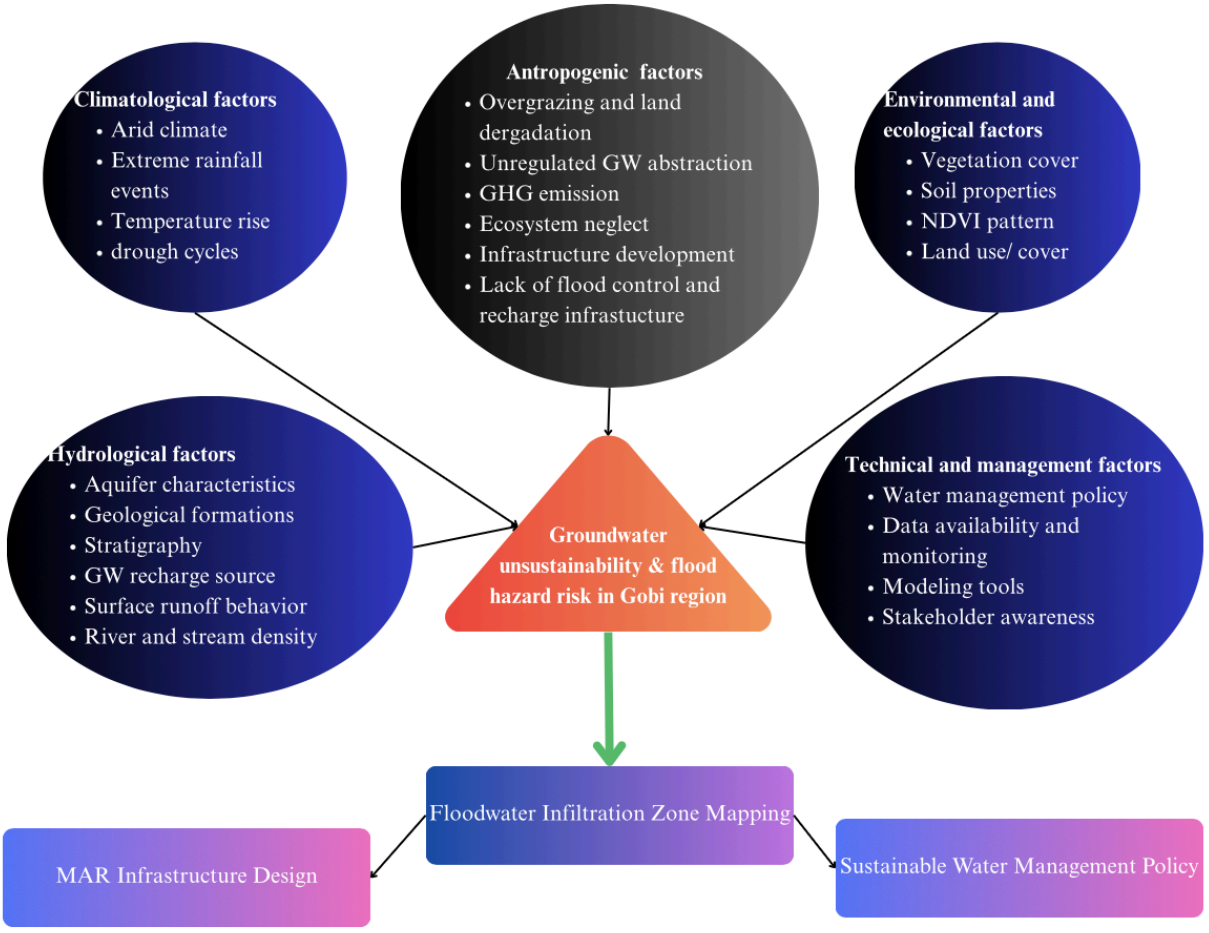

5. Conclusion and Recommendations

This section synthesizes the findings of the study and provides recommendations for the implementation of Managed Aquifer Recharge (MAR) technologies to address the challenges of flash floods and groundwater depletion in the study area, a region characterized by a dry climate where evaporation rates exceed precipitation. The study identified potential locations for converting floodwater into a valuable groundwater resource and estimated the potential volume of water that could be captured. Given the backdrop of unsustainable groundwater extraction by the mining industry and the

anticipated increase in water demand due to ongoing development, this approach holds significant promise for enhancing water security for the community.

The study's classification of the region based on its suitability for managed aquifer recharge revealed that a substantial portion, approximately 884.74 km² (51.1%), was classified as highly suitable. These areas exhibit a favorable overlap between surface water accumulation and infiltration potential, indicating a strong capacity for water to naturally seep into the ground. Moderately suitable zones covered 423.91 km² (24.5%), suggesting that with appropriate techniques, recharge could also be effective in these areas. Poorly suitable zones, primarily located in the northwestern and southern margins of the catchment, accounted for 288.02 km² (16.6%) and may require more specialized recharge methods. The remaining area was classified as very highly suitable (98.03 km²) and excellent suitability (35.04 km²), representing prime locations for maximizing recharge efficiency. The estimated volume of floodwater that could be captured for recharge was calculated to be 1,013,256.86 m³. This volume represents a potentially significant resource that is currently lost to evaporation or runoff.

In contrast, the main mining industry operating in the area consumes 485.1 liters per second from a deep, non-renewable aquifer with a total reserve estimated at 921.3 liters per second for the next 25 years, with no natural recharge occurring.While the long-term sustainability of this extraction rate remains uncertain, the non-renewable nature of the resource and the projected lifespan of the mining operation (over 50 years) underscore the potential for severe groundwater depletion.Furthermore, the region is expected to undergo development, leading to an inevitable increase in water demand from the community. The implementation of MAR, even if not directly utilized by the mining companies, can serve as a crucial compensation for the community, providing a sustainable source of water that would otherwise be lost to evaporation.

Based on the analysis, infiltration basins are recommended as a primary MAR technology for the highly suitable zones due to their potential for cost-effective recharge of large volumes of captured floodwater, given the favorable infiltration potential in these areas. For the poorly suitable zones and potentially for replenishing the deep aquifer used by the mining industry, injection wells (ASR) warrant further investigation. Diversion and retention structures along ephemeral streams could provide supplementary recharge by capturing peak flows during flash flood events. While offering a localized benefit, rainwater harvesting at the community level might have a limited overall impact due to the region's low rainfall. To further advance this work, several avenues of research are recommended. Expanding the criterion maps to

incorporate more detailed hydrogeological data will refine the suitability assessment for specific MAR technologies. Conducting pilot studies for infiltration basins and injection wells in representative zones will provide valuable data on their performance under local conditions, including clogging potential and water quality impacts. Detailed hydrogeological investigations are needed to better characterize the subsurface, particularly in areas where injection wells are being considered.

Reference

1. Bat-Erdene, Myagmarsuren, Munkhtsetseg Zorigt, Oyunbaatar Dambaravjaa, Dorjsuren Dechinlkhundev, Erdenesukh Sumiya, and Michael Nones. 2025. "Leveraging the GEV Model to Estimate Flood Due to Extreme Rainfall in Ungauged Dry Catchments of the Gobi Region" Sustainability 17, no. 6: 2500. https://doi.org/10.3390/su17062500.
2. Bayanzul, B., Nakamura, K., Machida, I. et al. Construction of a conceptual model for confined groundwater flow in the Gunii Khooloi Basin, Southern Gobi Region, Mongolia.Hydrogeol J 27, 1581–1596 (2019). https://doi.org/10.1007/s10040-019-01955-8
3. Tuinhof, A. and Buyanhisnig, N. 2010. Groundwater Assessment of the Southern Gobi Region. Mongolia Discussion Papers, East Asia and Pacific Sustainable Development Department. Washington, D.C.: World Bank.
4. Liu, Yesen, and Yaohuan Huang. 2020. "Why Flash Floods Occur Differently across Regions? A Spatial Analysis of China" Water 12, no. 12: 3344. https://doi.org/10.3390/w12123344
5. DRAFT INITIAL ENVIRONMENTAL EXAMINATION (IEE) REPORT - OMNOGOVI
6. Badarch, Ayurzana & Elbegjargal, Ariya & Dashjamts, Ariun-Erdene & Gansukh, Batzorig. (2021). Projected water demand by 2050 in South Gobi region of Mongolia. Proceedings of the Mongolian Academy of Sciences. 24-35. 10.5564/pmas.v61i03.1820.
7. Narantungalag, Odmaa. "Large-Scale Mining and Local Development: Evidence from Mongolia." Discussion Papers in Economics 21.01, School of Economics and Finance, Massey University, 2021. https://www.massey.ac.nz/documents/1309/DP21_01.pdf.IDEAS/RePEc+1Semantic Scholar+1
8. Williams, Martin. "Oyu Tolgoi: Impacts of Mining on Economic Outcomes in Mongolia." Harvard Kennedy School Faculty Research Working Paper Series RWP18-026, 2018. https://www.hks.harvard.edu/centers/mrcbg/publications/awp/awp126.

9. Dalaibuyan, B. (2022). Negotiating the coexistence of mining and pastoralism in Mongolia. *Journal of Contemporary East Asia Studies*, *11*(1), 46–63. https://doi.org/10.1080/24761028.2021.2021356
10. Mongolia: Human Settlements Development Program ,Development Oriented Aimag Plans – Volume 9, October 2022
11. Kovalenko, V.I., Yarmoluyk, V.V., Sal'nikova, E.B. et al. Geology, Geochronology, and Geodynamics of the Khan Bogd alkali granite pluton in southern Mongolia. Geotecton. 40, 450–466 (2006). https://doi.org/10.1134/S0016852106060033
12. Aloui, S., Zghibi, A., Mazzoni, A., Elomri, A., & Al-Ansari, T. (2024). Identifying suitable zones for integrated aquifer recharge and flood control in arid Qatar using GIS-based multi-criteria decision-making. *Groundwater for Sustainable Development, 25*, 101137. https://doi.org/10.1016/j.gsd.2024.101137
13. Mohan Lal, S.K. Mishra, Mukesh Kumar, Reverification of antecedent moisture condition dependent runoff curve number formulae using experimental data of Indian watersheds, CATENA, Volume 173, 2019, Pages 48-58, ISSN 0341-8162, https://doi.org/10.1016/j.catena.2018.09.002.
14. Farran, M.M., Elfeki, A.M. Evaluation and validity of the antecedent moisture condition (AMC) of Natural Resources Conservation Service-Curve Number (NRCS-CN) procedure in undeveloped arid basins. Arab J Geosci 13, 275 (2020). https://doi.org/10.1007/s12517-020-5242-y
15. Dillon, Peter & Alley, William & Zheng, Yan & Vanderzalm, Joanne & Ward, John & Megdal, Sharon & Hipke, Wesley & Thomas, Paul & Tuthill, David & Carlson, Ronald. (2022). Managed Aquifer Recharge: Overview and Governance.
16. Mingyuan Fan, Principal Water Resources Specialist Agriculture, Food, Nature, and Rural Development Sector Office, Sectors Group Asian Development Bank, Managed Aquifer Recharge in Mongolia: Policy Recommendations and Lessons Learned from Pilot Applications, OCTOBER 2023, https://www.adb.org/sites/default/files/publication/917341/adb-brief-263-managed-aquifer-recharge-mongolia.pdf
17. ICEM (International Centre for Environmental Management) and Asian Development Bank (ADB). 2020. Climate-Resilient Water Management in Mongolia: Policy Recommendations. Manila: ADB.
18. Heng Zhang, Yongxin Xu, Thokozani Kanyerere, A review of the managed aquifer recharge: Historical development, current situation and perspectives https://doi.org/10.1016/j.pce.2020.102887
19. Los Angeles County Department of Public Works. *Spreading Grounds Overview*. Accessed May 8, 2025. https://en.wikipedia.org/wiki/Spreading_ground.
20. Pyne, R.D.G. (1995). Groundwater Recharge and Wells: A Guide to Aquifer Storage Recovery (1st ed.). CRC Press. https://doi.org/10.1201/9780203719718
21. Boisson, A., Villesseche, D., Baisset, M. et al. Questioning the impact and sustainability of percolation tanks as aquifer recharge structures in semi-arid crystalline context. Environ Earth Sci 73, 7711–7721 (2015). https://doi.org/10.1007/s12665-014-3229-2

22. Heilweil, V.M. and Watt, D.E. (2011), Trench infiltration for managed aquifer recharge to permeable bedrock‡. Hydrol. Process., 25: 141-151. https://doi.org/10.1002/hyp.7833
23. Japan International Cooperation Agency (JICA). 2020. Gobi Desert Water Security Initiative. Tokyo: JICA.
24. Asian Development Bank (ADB). 2022. Ulaanbaatar Peri-Urban Recharge Project Report. Manila: ADB.
25. Intergovernmental Panel on Climate Change (IPCC). 2022. Climate Change 2022: Impacts, Adaptation and Vulnerability. Cambridge: Cambridge University Press.
26. Ministry of Environment and Green Development (MEGD), Mongolia. 2022. Mongolian Water Resource Assessment. Ulaanbaatar: MEGD.
27. National Water Committee. 2023. Flash Flood and Aquifer Suitability Analysis. Ulaanbaatar: Government of Mongolia.
28. United Nations Development Programme (UNDP). 2021. Traditional Water Systems and Climate Resilience in Mongolia. New York: UNDP.
29. World Bank. 2023. Kharkhorin Flood-MAR Pilot Evaluation. Washington, DC: World Bank Group.
30. Farhat, B., Souissi, D., Mahfoudhi, R. et al. GIS-based multi-criteria decision-making techniques and analytical hierarchical process for delineation of groundwater potential.Environ Monit Assess 195, 285 (2023). https://doi.org/10.1007/s10661-022-10845-8
31. Hossain, Md. Zahed, Sajal Kumar Adhikary, Hrithik Nath, Abdulla Al Kafy, Hamad Ahmed Altuwaijri, and Muhammad Tauhidur Rahman. 2024. "Integrated Geospatial and Analytical Hierarchy Process Approach for Assessing Sustainable Management of Groundwater Recharge Potential in Barind Tract" Water 16, no. 20: 2918. https://doi.org/10.3390/w16202918
32. Junze Zhang, Zhongqi Yu, Tengfei Yu, Jianhua Si, Qi Feng, Shixiong Cao,Transforming flash floods into resources in arid China,Land Use Policy,Volume 76,2018,Pages 746-753,ISSN 0264-8377,https://doi.org/10.1016/j.landusepol.2018.03.002.
33. M. M., Yagoub & Mahmoud, Sharaf. (2022). Application of Remote Sensing and Geographic Information System Techniques to Flood and Rainwater Harvesting: Case Study of Sennar, Sudan. DOI:10.1007/978-3-030-88874-9_14
34. Attwa, M., Ragab, D., El Bastawesy, M., Abd El-fattah, A.M. (2020). Flash Flood Management and Harvesting Via Groundwater Recharging in Wadi Systems: An Integrative Approach of Remote Sensing and Direct Current Resistivity Techniques. In: Negm, A. (eds) Flash Floods in Egypt. Advances in Science, Technology & Innovation. Springer, Cham. https://doi.org/10.1007/978-3-030-29635-3_7
35. Shruthi H Babu and D Sathish Kumar 2024 IOP Conf. Ser.: Earth Environ. Sci. 1326 012145 DOI 10.1088/1755-1315/1326/1/012145
36. Manoj K. Jain, Umesh C. Kothyari, Kittur G. Ranga Raju, A GIS based distributed rainfall–runoff model, Journal of Hydrology,Volume 299, Issues 1–2, 2004,Pages 107-135,ISSN 0022-1694, https://doi.org/10.1016/j.jhydrol.2004.04.024.
37. USDA Soil Conservation Service (SCS). 1985. National Engineering Handbook, Section 4: Hydrology. Washington, DC: USDA.

38. Kavzoglu, T., Tso, B., & Mather, P.M. (2024). Classification Methods for Remotely Sensed Data (3rd ed.). CRC Press. https://doi.org/10.1201/9781003439172
39. Mather, Paul M., and Magaly Koch. Computer processing of remotely-sensed images. John Wiley & Sons, 2022.https://doi.org/10.1002/9780470666517.fmatteropen_in_new
40. Yousif, M., Hussien, H.M. Flash floods mitigation and assessment of groundwater possibilities using remote sensing and GIS applications: Sharm El Sheikh, South Sinai, Egypt. Bull Natl Res Cent 44, 50 (2020). https://doi.org/10.1186/s42269-020-00307-x
41. Jha, Abhas K., Robin Bloch, and Jessica Lamond. 2012. Cities and Flooding: A Guide to Integrated Urban Flood Risk Management. Washington, DC: World Bank.
UNEP. 2021. Community-Based Early Warning Systems for Flash Floods in Arid Regions. Nairobi: United Nations Environment Programme. https://www.gfdrr.org/sites/default/files/publication/World_Bank_Cities_and_Flooding_Guidebook.pdf
42. SIVAPALAN, M., TAKEUCHI, K., FRANKS, S. W., GUPTA, V. K., KARAMBIRI, H., LAKSHMI, V., … ZEHE, E. (2003). IAHS Decade on Predictions in Ungauged Basins (PUB), 2003–2012: Shaping an exciting future for the hydrological sciences. Hydrological Sciences Journal, 48(6), 857–880. https://doi.org/10.1623/hysj.48.6.857.51421
43. Tao, Yixin, Bingwei Tian, Basanta Raj Adhikari, Qi Zuo, Xiaolong Luo, and Baofeng Di. 2024. "A Review of Cutting-Edge Sensor Technologies for Improved Flood Monitoring and Damage Assessment" Sensors 24, no. 21: 7090. https://doi.org/10.3390/s24217090
44. Allison, G. B., G. W. Gee, and S. W. Tyler. "Vadose‐zone techniques for estimating groundwater recharge in arid and semiarid regions." Soil Science Society of America Journal 58, no. 1 (1994): 6-14.
45. Famiglietti JS. The global groundwater crisis. *Nat Clim Chang.* 2014;4(11):945–8. doi:10.1038/nclimate2425.
46. Healy RW. *Estimating Groundwater Recharge*. Cambridge: Cambridge University Press; 2010.
47. Shaw EM, Beven KJ, Chappell NA, Lamb R. *Hydrology in Practice*. 4th ed. Boca Raton (FL): CRC Press; 2010.
48. IPCC. *Climate Change 2021: The Physical Science Basis*. Contribution of Working Group I to the Sixth Assessment Report of the Intergovernmental Panel on Climate Change. Cambridge: Cambridge University Press; 2021. doi:10.1017/9781009157896.
49. Taylor RG, Scanlon BR, Döll P, Rodell M, van Beek R, Wada Y, et al. Groundwater and climate change. *Nat Clim Chang.* 2013;3(4):322–9. doi:10.1038/nclimate1744.
50. Gleeson T, Wada Y, Bierkens MFP, van Beek LPH. Water balance of global aquifers revealed by groundwater footprint. *Nature.* 2012;488(7410):197–200. doi:10.1038/nature11295.
51. Scanlon BR, Ruddell BL, Reed PM, Hook RI, Zheng C, Tidwell VC, et al. The food-energy-water nexus: Transforming science for society. *Water Resour Res.* 2017;53(5):3550–6. doi:10.1002/2017WR020889.

52. Taylor RG, Scanlon BR, Döll P, Rodell M, van Beek R, Wada Y, et al. Groundwater and climate change. *Nat Clim Chang.* 2013;3(4):322–9. doi:10.1038/nclimate1744.
53. Famiglietti JS. The global groundwater crisis. *Nat Clim Chang.* 2014;4(11):945–8. doi:10.1038/nclimate2425.
54. Luigi Piemontese, Giulio Castelli, Ingo Fetzer, Jennie Barron, Hanspeter Liniger, Nicole Harari, Elena Bresci, Fernando Jaramillo, Estimating the global potential of water harvesting from successful case studies, Global Environmental Change, Volume 63, 2020, 102121, ISSN 0959-3780, https://doi.org/10.1016/j.gloenvcha.2020.102121.
55. Heng Zhang, Yongxin Xu, Thokozani Kanyerere, A review of the managed aquifer recharge: Historical development, current situation and perspectives, Physics and Chemistry of the Earth, Parts A/B/C, Volumes 118–119, 2020, 102887, ISSN 1474-7065, https://doi.org/10.1016/j.pce.2020.102887.
56. Sit, Muhammed, and Ibrahim Demir. "Decentralized flood forecasting using deep neural networks." arXiv preprint arXiv:1902.02308 (2019). https://doi.org/10.48550/arXiv.1902.02308
57. World Bank. *Water Security and the Sustainable Development Goals.* Washington (DC): World Bank; 2018. doi:10.1596/978-1-4648-1304-3.
58. UN-Water. *Policy Brief on Water and Climate Change.* Geneva: United Nations; 2020.
59. USDA Natural Resources Conservation Service. Soil Taxonomy: A Basic System of Soil Classification for Making and Interpreting Soil Surveys. 12th ed. Washington, DC: USDA; 2022
60. Zhenfeng Shao, Md. Enamul Huq, Bowen Cai, Orhan Altan, Yan Li,Integrated remote sensing and GIS approach using Fuzzy-AHP to delineate and identify groundwater potential zones in semi-arid Shanxi Province, China, Environmental Modelling & Software,Volume 134,2020,104868,ISSN 1364-8152, https://doi.org/10.1016/j.envsoft.2020.104868.
61. Machiwal, D., Rangi, N. & Sharma, A. Integrated knowledge- and data-driven approaches for groundwater potential zoning using GIS and multi-criteria decision making techniques on hard-rock terrain of Ahar catchment, Rajasthan, India. Environ Earth Sci 73, 1871–1892 (2015). https://doi.org/10.1007/s12665-014-3544-7
62. SARI, Dewi Novita, Alif Noor ANNA, Taryono TARYONO, Muchamad Farid MAULANA, and Dinda Nur Fadila KHUMAEROH. "DETECTION OF FLOOD HAZARD POTENTIAL ZONES BY USING ANALYTICAL HIERARCHY PROCESS IN TUNTANG WATERSHED AREA, INDONESIA." Geographia Technica 19, no. 1 (2024).. J Environ Manage. 2023;330:117137. DOI: 10.21163/GT_2024.191.05
63. Souissi, D., Msaddek, M. H., Zouhri, L., Chenini, I., El May, M., & Dlala, M. (2018). Mapping groundwater recharge potential zones in arid region using GIS and Landsat approaches, southeast Tunisia. Hydrological Sciences Journal, 63(2), 251–268. https://doi.org/10.1080/02626667.2017.1414383
64. Loritz, R., Hrachowitz, M., Neuper, M., and Zehe, E.: The role and value of distributed precipitation data in hydrological models, Hydrol. Earth Syst. Sci., 25, 147–167, https://doi.org/10.5194/hess-25-147-2021, 2021.

65. Anderson JR, Hardy EE, Roach JT et al. A Land Use and Land Cover Classification System for Use with Remote Sensor Data. USGS Professional Paper 964. Reston, VA: USGS; 2021
66. U.S. Department of Agriculture, Natural Resources Conservation Service. National Engineering Handbook, Part 630: Hydrology. Chapter 9: Hydrologic Soil-Cover Complexes. Washington, DC: USDA NRCS; 2004.
67. U.S. Department of Agriculture, Natural Resources Conservation Service. Urban Hydrology for Small Watersheds. Technical Release 55. Washington, DC: USDA NRCS; 1986.
68. U.S. Department of Agriculture, Natural Resources Conservation Service. National Engineering Handbook, Part 630: Hydrology. Chapter 7: Hydrologic Soil Groups. Washington, DC: USDA NRCS; 2007.
69. Shangguan W, Hengl T, Mendes de Jesus J, Yuan H, Dai Y. Mapping the global depth to bedrock for land surface modeling. J Adv Model Earth Syst. 2017;9(1):65–88.
70. Oyu Tolgoi LLC. Year in Review 2023. Ulaanbaatar: Oyu Tolgoi LLC; 2023 [cited 2025 May 2]. Available from: https://admin.ot.mn/wp-content/uploads/Year_in_Review_2023_EN.pdfOT Data
71. Rio Tinto. Oyu Tolgoi Communities. London: Rio Tinto; [cited 2025 May 2]. Available from: https://www.riotinto.com/en/operations/mongolia/oyu-tolgoi/oyu-tolgoi-communitiesRio Tinto+1Rio Tinto+1
72. Rawls WJ, Brakensiek DL, Saxtonn KE. Estimation of soil water properties. Transactions of the ASAE. 1983;25(5):1316–1320.
73. FAO. World reference base for soil resources. Rome: Food and Agriculture Organization of the United Nations; 1998. Report No.: FAO World Soil Resources Report 84.
74. Chow VT, Maidment DR, Mays LW. Applied Hydrology. New York: McGraw-Hill; 2013.

Appendixes

1. Daily precipitation from 2010- 2024

Available on the drive link: meteo data of the region

2. IDF curves

Pivot conversion

Row Labels	Max of H72	Max of H144	Max of H216	Max of H288	Max of H360	Max of H432	Max of H504	Max of H576	Max of H648	Max of H720
2010	54.6	54.6	60	60.9	75	77.1	77.7	78	78.6	78.6
2011	40.8	45.3	46.2	49.5	49.5	55.8	58.2	58.2	77.7	83.7
2012	113.1	150	151.8	155.7	175.2	177.9	177.9	177.9	177.9	177.9
2013	59.1	59.4	60	60	60	63	63.3	116.1	116.7	117
2014	48	56.1	57.3	59.7	59.7	63.3	63.3	63.3	76.2	84
2015	41.7	48	54.9	54.9	60	60	70.5	71.4	71.7	71.7
2016	38.1	49.8	68.4	69.6	83.4	85.8	85.8	85.8	85.8	85.8
2017	1.137	1.677	1.905	1.905	1.965	1.965	1.965	1.965	2.097	2.097
2018	3.978	4.998	5.919	6.132	6.132	6.432	6.432	6.432	6.909	7.122
2019	1.587	1.857	1.881	2.022	2.163	2.235	2.235	2.235	2.235	2.235
2020	5.046	5.142	5.202	5.298	5.781	5.877	5.877	5.973	6.21	6.282
2021	3.168	4.482	4.83	4.842	4.842	4.842	4.842	4.842	4.842	5.595
2022	8.7	8.7	9.3	9.3	9.3	9.3	12	12	12	12
2023	32.7	57	57.3	57.6	57.9	58.2	58.2	58.2	63	63.3
2024	42.6	46.2	46.2	46.2	48	48.9	51.3	54.9	54.9	54.9
Grand Total	113.1	150	151.8	155.7	175.2	177.9	177.9	177.9	177.9	177.9

Row Labels	Max of 24h	Max of H48	Max of H72	Max of H96	Max of H192	Max of H360	Max of H432
2010	18.2	18.2	20	20.3	26	28.1	46.2
2011	13.6	15.1	15.4	16.5	19.4	29.3	30.7
2012	37.7	50	50.6	51.9	59.3	60	64.1
2013	19.7	19.8	20	20	38.7	40	41.9
2014	16	18.7	19.1	19.9	21.1	28	30.6
2015	13.9	16	18.3	18.3	23.8	24.5	24.5

2016	**12.7**	**16.6**	**22.8**	**23.2**	**28.6**	**36.1**	**40.4**
2017	**0.379**	**0.559**	**0.635**	**0.635**	**0.655**	**0.699**	**0.75**
2018	**1.326**	**1.666**	**1.973**	**2.044**	**2.144**	**2.474**	**2.65**
2019	**0.529**	**0.619**	**0.627**	**0.674**	**0.745**	**0.761**	**0.773**
2020	**1.682**	**1.714**	**1.734**	**1.766**	**1.991**	**2.133**	**2.202**
2021	**1.056**	**1.494**	**1.61**	**1.614**	**1.614**	**1.981**	**2.065**
2022	**2.9**	**2.9**	**3.1**	**3.1**	**4**	**4**	**4**
2023	**10.9**	**19**	**19.1**	**19.2**	**19.4**	**21.5**	**21.7**
2024	**14.2**	**15.4**	**15.4**	**15.4**	**18.3**	**19.6**	**20.2**
Grand Total	**37.7**	**50**	**50.6**	**51.9**	**59.3**	**60**	**64.1**

	H24	H48	H72	H96	H192	H360	H432
Avr	10.9848	13.18346667	14.02526667	14.3022	17.7166	19.9432	22.18266667
StDev	10.21580901	12.93029148	13.3317729	13.64070934	16.74894694	17.82386854	20.07358793

	24	48	72	96	192	360	432
Avr	0.4577	0.274656	0.194795	0.148981	0.092274	0.055398	0.051349
StDev	0.425659	0.269381	0.185164	0.142091	0.087234	0.049511	0.046467

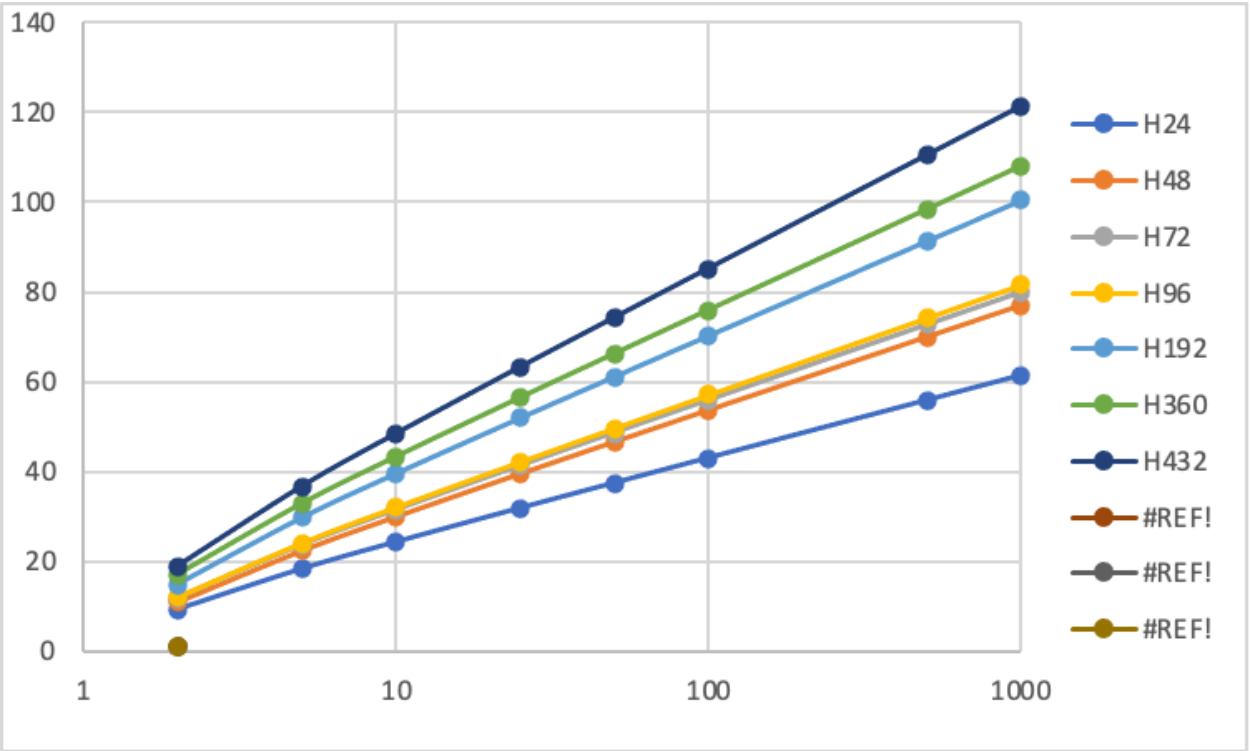

KT	Return period	H24	H48	H72	H96	H192	H360	H432
-0.164	2	9.305777001	11.05830392	11.83411829	12.06027626	14.96382075	17.01375162	18.88346484
0.720	5	18.3383675	22.49097928	23.62177457	24.12108725	29.7728661	32.77321867	36.63208361
1.305	10	24.31872836	30.06040516	31.42622871	32.10639357	39.5777427	43.20735714	48.38321359
2.045	25	31.87493016	39.62439482	41.2871772	42.19584927	51.96623028	56.39091876	63.23079748
2.594	50	37.48055231	46.71950871	48.6025921	49.68078387	61.15671807	66.17123789	74.24558338
3.138	100	43.04478343	53.76223338	55.86399113	57.1104509	70.27934473	75.87934067	85.17903784
4.397	500	55.90287211	70.03689498	72.64397578	74.27927719	91.36034232	98.31328419	110.444582
4.938	1000	61.43074133	77.0335959	79.85792202	81.66039181	100.4233532	107.9579451	121.306587

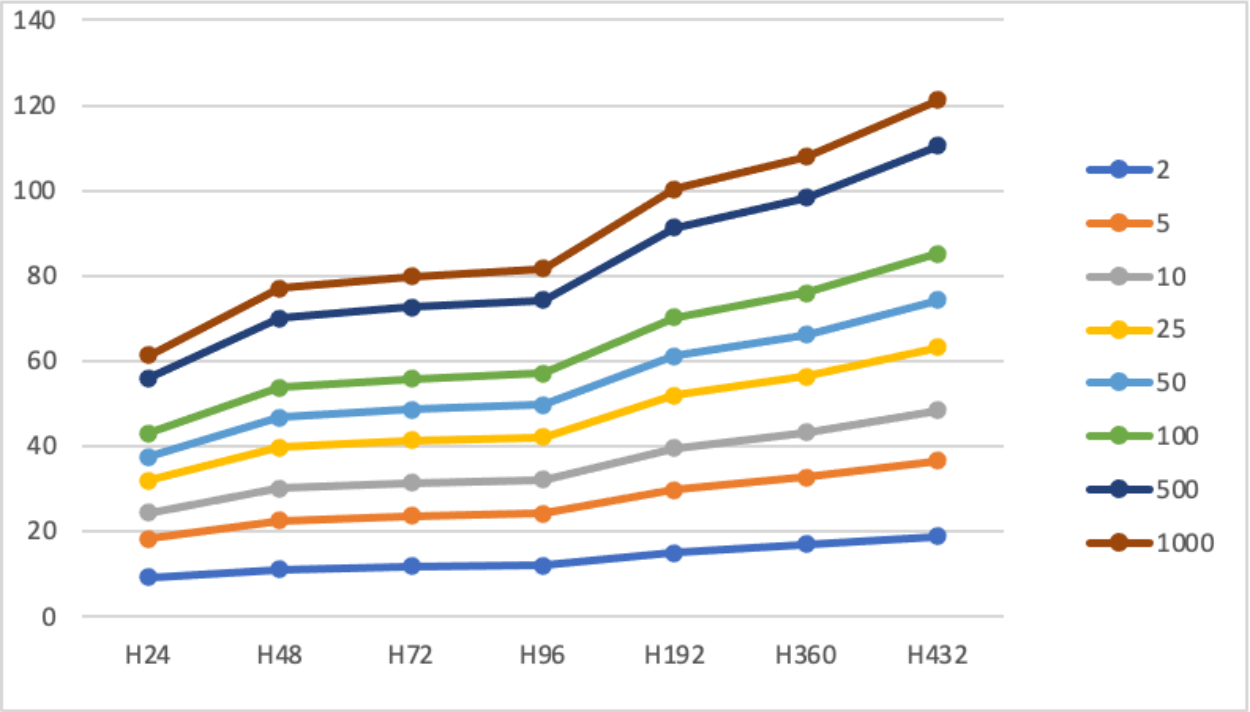

Return period	x24	x48	x72	x96	x192	x360	x432
2	0.387741	0.230381	0.164363	0.125628	0.077937	0.04726	0.043712
5	0.764099	0.468562	0.32808	0.251261	0.155067	0.091037	0.084796
10	1.01328	0.626258	0.436475	0.334442	0.206134	0.12002	0.111998
25	1.328122	0.825508	0.573433	0.43954	0.270657	0.156641	0.146368
50	1.56169	0.973323	0.675036	0.517508	0.318525	0.183809	0.171865
100	1.793533	1.120047	0.775889	0.594901	0.366038	0.210776	0.197174
500	2.329286	1.459102	1.008944	0.773742	0.475835	0.273092	0.255659
1000	2.559614	1.604867	1.109138	0.850629	0.523038	0.299883	0.280802

3. QGIS

Corresponding data available in drive link: QGIS

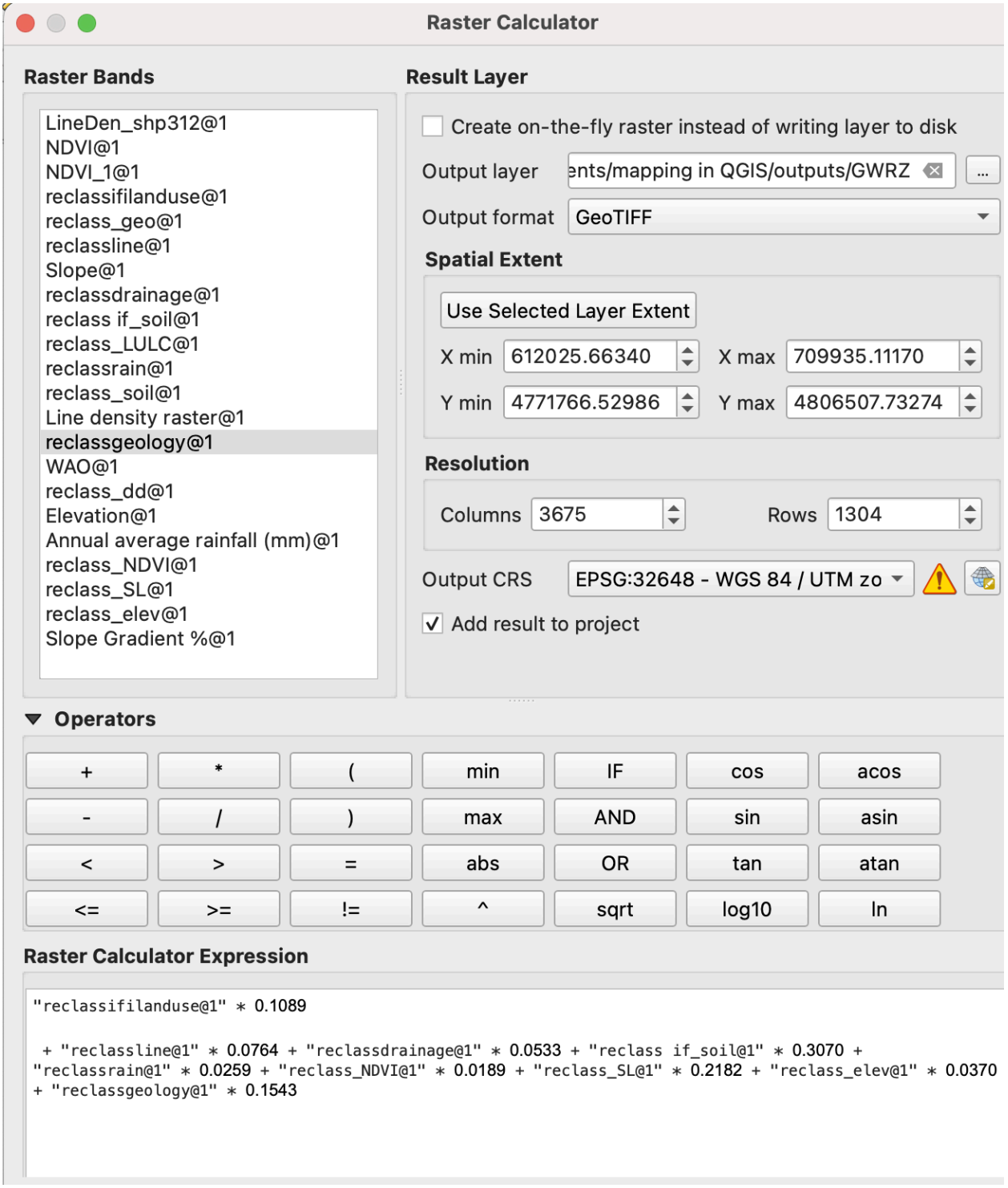
Raster Calculator
Raster Bands
LineDen_shp312@1
NDVI@1
NDVI_1@1
reclassifilanduse@1
reclass_geo@1
reclassline@1
Slope@1
reclassdrainage@1
reclass if_soil@1
reclass_LULC@1
reclassrain@1
reclass_soil@1
Line density raster@1
reclassgeology@1
WAO@1
reclass_dd@1
Elevation@1
Annual average rainfall (mm)@1
reclass_NDVI@1
reclass_SL@1
reclass_elev@1
Slope Gradient %@1
Result Layer
Create on-the-fly raster instead of writing layer to disk
Output layer
ents/mapping in QGIS/outputs/GWRZ
...
Output format
GeoTIFF
Spatial Extent
Use Selected Layer Extent
X min
612025.66340
X max
709935.11170
Y min
4771766.52986
Y max
4806507.73274
Resolution
Columns
3675
Rows
1304
Output CRS
EPSG:32648 - WGS 84 / UTM zo
Add result to project
Operators
+
*
(
min
IF
cos
acos
-
/
)
max
AND
sin
asin
<
>
=
abs
OR
tan
atan
<=
>=
!=
^
sqrt
log10
ln
Raster Calculator Expression
"reclassifilanduse@1" * 0.1089
+ "reclassline@1" * 0.0764 + "reclassdrainage@1" * 0.0533 + "reclass if_soil@1" * 0.3070 +
"reclassrain@1" * 0.0259 + "reclass_NDVI@1" * 0.0189 + "reclass_SL@1" * 0.2182 + "reclass_elev@1" * 0.0370
+ "reclassgeology@1" * 0.1543

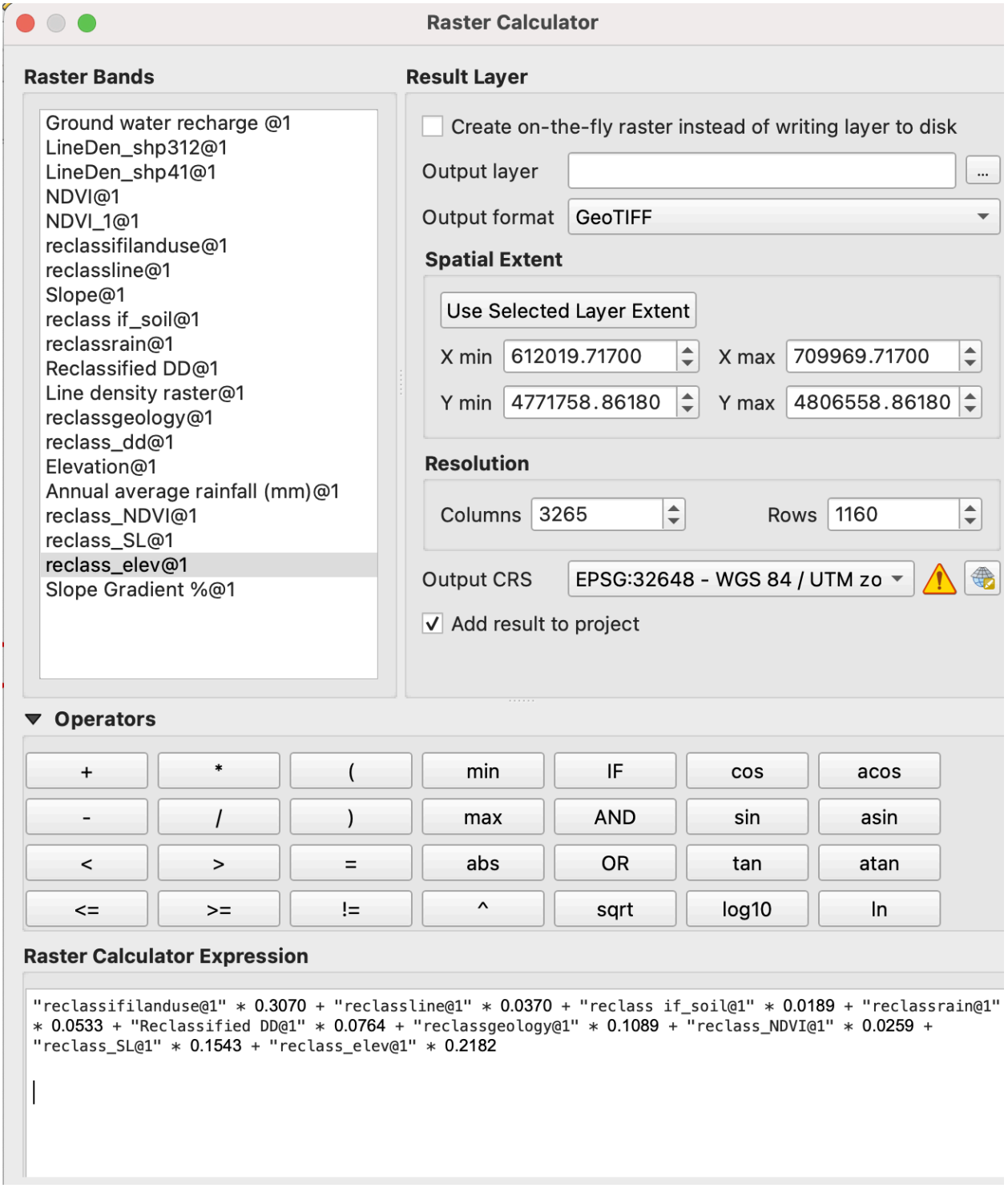
Raster Calculator
Raster Bands
Ground water recharge @1
LineDen_shp312@1
LineDen_shp41@1
NDVI@1
NDVI_1@1
reclassifilanduse@1
reclassline@1
Slope@1
reclass if_soil@1
reclassrain@1
Reclassified DD@1
Line density raster@1
reclassgeology@1
reclass_dd@1
Elevation@1
Annual average rainfall (mm)@1
reclass_NDVI@1
reclass_SL@1
reclass_elev@1
Slope Gradient %@1
Result Layer
Create on-the-fly raster instead of writing layer to disk
Output layer
...
Output format
GeoTIFF
Spatial Extent
Use Selected Layer Extent
X min
612019.71700
X max
709969.71700
Y min
4771758.86180
Y max
4806558.86180
Resolution
Columns
3265
Rows
1160
Output CRS
EPSG:32648 - WGS 84 / UTM zo
Add result to project
Operators
+
*
(
min
IF
cos
acos
-
/
)
max
AND
sin
asin
<
>
=
abs
OR
tan
atan
<=
>=
!=
^
sqrt
log10
ln
Raster Calculator Expression
"reclassifilanduse@1" * 0.3070 + "reclassline@1" * 0.0370 + "reclass if_soil@1" * 0.0189 + "reclassrain@1" * 0.0533 + "Reclassified DD@1" * 0.0764 + "reclassgeology@1" * 0.1089 + "reclass_NDVI@1" * 0.0259 + "reclass_SL@1" * 0.1543 + "reclass_elev@1" * 0.2182